SECRET

WT-1436

This document consists of 68 pages.
No. 162 of 192 copies, Series A

OPERATION PLUMBBOB

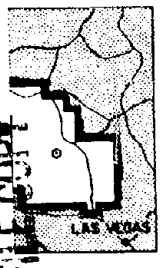

NEVADA TEST SITE
MAY–OCTOBER 1957

Project 6.2

MEASUREMENT OF THE MAGNETIC COMPONENT OF THE ELECTROMAGNETIC FIELD NEAR A NUCLEAR DETONATION (U)

Issuance Date: May 8, 1962

HEADQUARTERS FIELD COMMAND
DEFENSE ATOMIC SUPPORT AGENCY
SANDIA BASE, ALBUQUERQUE, NEW MEXICO

SECRET

Inquiries relative to this report may be made to

Chief, Defense Atomic Support Agency
Washington 25, D. C.

When no longer required, this document may be destroyed in accordance with applicable security regulations.

DO NOT RETURN THIS DOCUMENT

USAEC Division of Technical Information Extension, Oak Ridge, Tennessee

SECRET

WT-1436

OPERATION PLUMBBOB—PROJECT 6.2

MEASUREMENT OF THE MAGNETIC COMPONENT OF THE ELECTROMAGNETIC FIELD NEAR A NUCLEAR DETONATION (U)

P.H. Haas, Project Officer
F.N. Wimenitz, Asst. Project Officer
J.C. Hoadley
J.S. Wicklund

Diamond Ordnance Fuze Laboratories
Washington 25, D.C.

SECRET

ABSTRACT

The magnetic component of the electromagnetic field generated by several nuclear detonations during Operation Plumbbob was measured at distances ranging from 650 to 14,400 feet from ground zero. The output from low-impedance, shielded-loop antennas was amplified, in some cases integrated, and then recorded on magnetic tape by specially designed, ruggedized, and well-shielded tape recorders.

Oscillographic representations obtained from the tapes upon playback include records of field intensity versus time and the time derivative of field intensity versus time. It was determined that the major component of the field is in the azimuthal direction H_{ϕ}, and that relatively strong vertical and radial fields also exist. Initially sharply rising fields, lasting no longer than 100 msec are followed by longer persistence signals with rise times of millisecond order.

FOREWORD

This report presents the final results of one of the 46 projects comprising the military-effect programs of Operation Plumbbob, which included 24 test detonations at the Nevada Test Site in 1957.

For overall Plumbbob military-effects information, the reader is referred to the "Summary Report of the Director, DOD Test Group (Programs 1--9)," ITR--1445, which includes: (1) a description of each detonation, including yield, zero-point location and environment, type of device, ambient atmospheric conditions, etc.; (2) a discussion of project results; (3) a summary of the objectives and results of each project; and (4) a listing of project reports for the military-effect program.

PREFACE

Messrs. J.D. Rosenberg and K.D. Zastrow guided the majority of the tape recorder electronics designs. Mr. R. Puttcamp designed the preamplifiers and integrators and was responsible for most of the oscillograms in the field. Mr. A. Hill designed and built the playback recorder and also prepared the oscillograms used in this report. Mr. B. Lackey was responsible for logistics and direction of the field installation and recovery crew. Mr. A.G. McNish, then Consultant to the Director, National Bureau of Standards, performed most of the calculations used in Section 1.3, as well as served as consultant to the project. To all these, who contributed freely of their time, the authors express their appreciation.

CONTENTS

ABSTRACT ---- 5

FOREWORD ---- 6

PREFACE ---- 6

CHAPTER 1 INTRODUCTION ---- 11

1.1 Objective ---- 11
1.2 Background ---- 11
1.2.1 Army Requirements ---- 11
1.2.2 Results from Previous Projects ---- 11
1.3 Theory ---- 12
1.3.1 Coordinates and Dipole Moment ---- 12
1.3.2 Fourier Representation ---- 12
1.3.3 Electric Field ---- 13
1.3.4 Relations between Electric and Magnetic Fields ---- 13
1.3.5 Calculations ---- 14
1.3.6 Effect of Distance on Spectrum ---- 14

CHAPTER 2 PROCEDURE ---- 17

2.1 Recording Equipment ---- 17
2.1.1 System Design ---- 18
2.1.2 Magnetic Shielding ---- 18
2.1.3 Antenna System ---- 19
2.1.4 Recording System ---- 20
2.1.5 Magnetic Heads ---- 21
2.1.6 HF/AC Bias Requirement Determination ---- 22
2.1.7 Tape Transport ---- 23
2.1.8 Electronics ---- 24
2.1.9 Power Supply ---- 25
2.1.10 Recorder Package ---- 26
2.2 Calibration ---- 26
2.3 Method of Installation and Recovery ---- 26
2.4 Station Locations ---- 27
2.5 Data Requirements and Analysis ---- 27

CHAPTER 3 RESULTS ---- 45

3.1 Degree of Successful Participation ---- 45
3.1.1 Shot Lassen ---- 45
3.1.2 Shot Wilson ---- 45
3.1.3 Shot Priscilla ---- 45
3.1.4 Shot Hood ---- 45
3.1.5 Shot Diablo ---- 45
3.1.6 Shot Owens ---- 45
3.2 Discussion of Data ---- 46
3.3 Presentation of Data ---- 46

3.3.1 Introduction ---- 46
3.3.2 General Description of Signals ---- 46
3.4 Analysis of Data ---- 47
3.4.1 Introduction ---- 47
3.4.2 Scaling Laws ---- 47

CHAPTER 4 CONCLUSIONS AND RECOMMENDATIONS ---- 64

4.1 Conclusions ---- 64
4.2 Recommendations ---- 64

REFERENCES ---- 65

TABLES

2.1 Recorder Event Sequence ---- 28
2.2 Slant Ranges of Stations ---- 28
3.1 Summary of Amplitudes of First Peaks, H_ϕ ---- 49
3.2 Summary of Amplitudes of First Peaks, dH_ϕ/dt ---- 50
3.3 Summary of Amplitudes of First Peaks, H_r and H_z ---- 50
3.4 Summary of Amplitudes of First Peaks, dH_r/dt and dH_z/dt ---- 51
3.5 Participation and Oscillogram Reference, Shot Priscilla ---- 51
3.6 Participation and Oscillogram Reference, Shot Hood ---- 52
3.7 Participation and Oscillogram Reference, Shot Owens ---- 52
3.8 Participation and Oscillogram Reference, Shot Wilson ---- 52

FIGURES

1.1 Predicted magnetic field intensity versus time ---- 16
1.2 Predicted derivative of magnetic field intensity versus time ---- 16
1.3 Ratio of field intensities versus distance and frequency ---- 16
2.1 Instrumentation system package ---- 29
2.2 Loop antenna ---- 30
2.3 Block diagram of instrumentation system ---- 31
2.4 7-channel magnetic head ---- 32
2.5 View of tape transport, showing armored tape compartment and timer ---- 32
2.6 Top view of tape transport showing tape path ---- 33
2.7 Tape recorder plug-in units ---- 33
2.8 Schematic of high-band integrator ---- 34
2.9 Schematic of low-band integrator ---- 34
2.10 Schematic of FM modulator, HF band ---- 35
2.11 Schematic of FM modulator, LF band ---- 35
2.12 Schematic of mixer filter ---- 36
2.13 Schematic of timing oscillator and cathode follower ---- 36
2.14 Schematic of high-band preamplifier 1 ---- 37
2.15 Schematic of high-band preamplifier 2 ---- 37
2.16 Schematic of low-band preamplifier ---- 38
2.17 Schematic of recorder electronics ---- 39
2.18 Recorder, inside view ---- 40
2.19 Recorder, end view ---- 40
2.20 Recorder, side view ---- 41
2.21 Recorder, side view ---- 41
2.22 Recorder package being transferred from service area to outer magnetic shield box ---- 42
2.23 Lowering recorder package into magnetic shield box ---- 42

2.24 Lowering recording package into hole ---------- 43
2.25 Station locations ---------- 44
3.1 Oscillograms of H and dH/dt versus time, Shot Priscilla ---------- 53
3.2 Oscillograms of H and dH/dt versus time, Shot Hood ---------- 54
3.3 Oscillograms of H and dH/dt versus time, Stations .02 and .03, Shot Hood ---------- 55
3.4 Oscillograms of H and dH/dt versus time, Stations .04 and .05, Shot Hood ---------- 56
3.5 Oscillograms of H and dH/dt versus time, Shot Owens ---------- 57
3.6 Oscillograms of H and dH/dt versus time, Shot Wilson ---------- 58
3.7 Oscillograms of H and dH/dt versus time, Shots Diablo and Lassen ---------- 59
3.8 Normalized amplitudes versus slant range, H_ϕ ---------- 60
3.9 Normalized amplitudes versus slant range, dH_ϕ/dt ---------- 61
3.10 Normalized amplitudes versus slant range, dH_r/dt ---------- 62
3.11 Normalized amplitudes versus slant range, dH_z/dt ---------- 63

Chapter 1

INTRODUCTION

1.1 OBJECTIVE

The objective was to provide a record of the magnetic-field component of the electromagnetic field from a nuclear detonation as a function of time and distance, including the near-field region. This specifically includes distances sufficiently removed from the detonation point to assure little or no physical damage to an antitank mine and fuze, and the maximum distance at which mine clearance (by sympathetic fuze function) is possible by a nuclear weapon.

1.2 BACKGROUND

1.2.1 Army Requirements. The Mine Fuze Branch of the Diamond Ordnance Fuze Laboratories (DOFL) is engaged in research and development of influence mine fuzes for use with antitank mines. Influence mine fuzes use a variety of signals to sense the presence of their intended target. Use is sometimes made of combinations of such signals and of the specific sequences in which they occur for fuze function. Some of the signals emanate from the target itself, others are target-produced changes in ambient conditions, and still others originate with the fuze and are reflected by the target; all are detected by suitable sensing devices within the fuze. Vibration of the ground, changes in the ambient magnetic field, and reflected nuclear radiation (from appropriate sources associated with the mine fuze) are examples of such influences.

A particular influence mine fuze presently in the production engineering stage uses a combination of seismic and magnetic influences. It is necessary to ascertain whether the variations in the magnetic field from an atomic detonation are of such nature as to (1) cause the mine fuze to detonate or (2) alter the fuze's sensing mechanism so as to change its sensitivity (this could be an increase as well as a decrease). It also appears that data on the magnitude and nature of the electromagnetic fields in the close vicinity of nuclear detonations will be of value to the designers of (1) more elaborate ground installations containing active electronic instrumentation that has to survive close to, during, and immediately after the detonation, as well as (2) electronic guidance and fuzing circuits and missiles.

1.2.2 Results from Previous Projects. Electromagnetic measurements have been conducted during previous operations, principally by Los Alamos Scientific Laboratory (LASL), (References 1 and 2); AFOAT-1, (Reference 3); and Signal Corps Engineering Laboratories (SCEL), (Reference 4). Values of the electric field component at distances upward of 20 km were obtained. LASL was concerned mainly with the first few microseconds of the signal for diagnostic purposes, AFOAT-1 and SCEL with approximately the first 100 μsec, mostly at much greater distances. Reference 2 and discussions with its authors indicate the probable existence of signals with periods up to 2 seconds.

1.3 THEORY

The prompt signal is generally considered to be due to Compton electrons produced by gamma rays emitted during the detonation (References 5 and 6). When conditions are such that asymmetries are produced in the expanding sphere of Compton electrons and associated ionization electrons, an electromagnetic pulse is produced. Pulses predicted by theories based on such considerations, however, have durations too short to agree with observation; the longer times actually observed are held by some to be due to electron attachment to neutral O_2 molecules (Reference 6).

The extremely low frequency signals, as reported in Reference 2, are still poorly understood. Many investigators feel this phenomenon is associated with the expansion of the ball of ionized gas in the earth's magnetic field, but as yet no reports have been published on this subject.

All previously recorded data indicates that the source of the electromagnetic signal may, at least at large distances from ground zero, be represented by a vertical electric dipole. Even for distances of a few thousand yards, experiments on induced ground currents (Reference 7) support this conclusion, except that this evidence does not preclude the existence of higher-order multipole sources of lower energy in addition to the dipole source. Calculations of predicted field strengths were, therefore, made on the basis of a vertical-dipole source with the distinct understanding that the measurements would include attempts to establish or disprove the existence of field components that do not arise from such a source.

1.3.1 Coordinates and Dipole Moment. The spherical coordinates used are radial r, polar angle θ, and azimuthal ϕ. The plane $\theta = \pi/2$ is taken as an interface between a perfectly conducting medium $\theta > \pi/2$ and an insulating medium of dielectric constant ϵ_0 and permeability μ_0 $(\theta < \pi/2)$. If there is a displacement of charge q along the vertical axis a distance $l/2$, there will be a corresponding displacement of charge from the interface equivalent to displacement of charge $-q$ to a distance of $-l/2$. Thus, the displaced charge and its image may be regarded as a vertical electric dipole of moment $P = ql$ whose strength is measured in coulomb meters.

1.3.2 Fourier Representation. If the displacement of charge takes place in a finite time, the value of $P = f(t)$ is given by a Fourier integral:

$$P_t = \int_{-\infty}^{\infty} q(\omega)\, e^{i\omega t}\, d\omega \tag{1.1}$$

However, if the duration of the displacement is sufficiently short so that the values of P and of its time derivatives are insignificantly different from zero at some time after the initiation of the displacement, the values of P_t may be represented to any required degree of precision over this interval by a Fourier series. This is equivalent to assuming that the charge displacement is repeated at intervals of τ, but this does not impair the accuracy of the representation, provided frequencies lying between zero and $1/\tau$ are not considered. In this case the electric dipole moment will be given by

$$P_t = \sum_{0}^{n} [A_n \cos 2\pi n(t/\tau) + B_n \sin 2\pi n (t/\tau)] \tag{1.2}$$

Where: A_n, B_n = magnitudes of Fourier components, coulomb meters

t = time from arbitrary origin, seconds

τ = time interval over which the representation is to be given, seconds.

As stated before, τ is selected to be sufficiently long that P_t and its time derivatives are

essentially zero at its bounds. If the charge displacement begins sharply, it is convenient to set $t = 0$ at this time, or just before it.

This finite-series representation can be made to approach the integral as closely as desired by extension of the interval τ and the increasing of n. In the finite representation, A_n and B_n are approximations to the contributions to P_f due to the spectral contributions lying between $(n - \frac{1}{2})/\tau$ and $(n + \frac{1}{2})/\tau$ in the integral representation. As τ and n approach infinity, A_n and B_n approach the spectral density at the frequency $f = n/\tau$ in the even and odd components of the integral representation.

1.3.3 Electric Field. The θ component of the electric field at the interface, a distance r from the origin due to the charge displacement is given by:

$$E_\theta = \frac{1}{4\pi\epsilon} \sum \left[A_n \left(\frac{\cos 2\pi n t^*}{r^3} - \frac{2\pi n \sin 2\pi n t^*}{\tau c r^2} - \frac{4\pi^2 n^2 \cos 2\pi n t^*}{\tau^2 c^2 r} \right) + B_n \left(\frac{\sin 2\pi n t^*}{r^3} - \frac{2\pi n \cos 2\pi n t^*}{\tau c r^2} - \frac{4\pi^2 n^2 \sin 2\pi n t^*}{\tau^2 c^2 r} \right) \right] \quad (1.3)$$

Where: $t^* = t/\tau - r/\tau c$

The equation shows that each frequency component in the charge displacement is represented by a corresponding component in the electric-field changes. The contributions to the field involving $1/r^3$ (the quasi-static term) are of the same relative strengths, term for term, that they are in the source function. The contributions involving $1/r^2$ (the induction term) are relatively enhanced by a factor of n with respect to their relative strengths in the source, while the contributions involving $1/r$ (the radiation term) are relatively enhanced by a factor of n^2.

The concern here is with observations of the electric field at distances where the contributions involving $1/r^3$ and $1/r^2$ are important for the lower frequency terms; hence, attention cannot be confined to the radiation field.

1.3.4 Relations between Electric and Magnetic Fields. The notations in the preceding section, which were designed to facilitate numerical calculation, are cumbersome for theoretical discussion. In examining the relationship between the electric and magnetic fields, it can be assumed that the source is a simple harmonic, and the equations for the electric and magnetic fields at the interface can be written in the form:

$$E_\theta = \frac{1}{4\pi\epsilon_\theta} \left(\frac{1}{r^3} + \frac{i\omega}{cr^2} - \frac{\omega^2}{c^2 r} \right) |P| e^{-i\omega t^*} \quad (1.4)$$

$$H_\phi = \frac{1}{4\pi} \left(\frac{i\omega}{r^2} - \frac{\omega^2}{cr} \right) |P| e^{-i\omega t^*} \quad (1.5)$$

Furthermore:

$$\frac{dB_\psi}{dt} = \frac{\mu_0}{4\pi} \left(\frac{\omega^2}{r^2} + \frac{i\omega^3}{cr} \right) |P| e^{-i\omega t^*} \quad (1.6)$$

At very great distances, only the terms in $1/r$ are important, and the impedance reduces to the well-known quantity 120π ohms, i.e., the electric field in volts per meter has approximately 377 times the numerical value of the magnetic field in ampere turns per meter. This, however, does not hold true for regions where terms in $1/r^3$ and $1/r^2$ are important. Taking the ratio of E_θ to H_ϕ, the following complex value is obtained:

$$\frac{E_\theta}{H_\phi} = \sqrt{\frac{\mu_0}{\epsilon_0}} \left(\frac{1}{1 + \frac{\lambda^2}{4\pi^2 r^2}} - i \frac{1}{\frac{8\pi^3 r^3}{\lambda^3} + \frac{2\pi r}{\lambda}} \right) \tag{1.7}$$

Where: λ = wave length, meters.

For the radiation field region where terms in 1/r predominate in Equations 1.4 and 1.5 ($r \gg \lambda$), Equation 1.7 reduces to $\sqrt{\mu_0/\epsilon_0}$ or 120π, and E and H are in phase. While for the near field here under consideration ($r \ll \lambda$):

$$\frac{E_\theta}{H_\phi} = -i \sqrt{\frac{\mu_0}{\epsilon_0}} \frac{\lambda}{2\pi r} \tag{1.8}$$

that is, the fields are in phase quadrature and the numerical value of the electric field in volts per meter is much larger than that of the magnetic field in ampere turns per meter. For intermediate ranges, this ratio then decreases and has a more complex phase relationship.

1.3.5 Calculations. A number of electromagnetic pulses have been accurately observed at known distances from the charge displacements giving rise to them. Since the source was approximately 20 km from the point of observation and since there were important contributions to the pulses in the frequency range below a few kilocycles, the quasi-static and induction terms were both important. Shot 7 of Operation Upshot-Knothole was selected as having a typical pulse height and frequency spectrum. The predominant frequency at 17.8 km was estimated to be 14 kc, and the approximate total pulse duration 54 μsec (Reference 3, Table 4.1). The dipole moment contributions to a number of frequencies (per kilocycle band width) were calculated, and the electric magnetic fields due to these dipole moments were synthesized by the use of the equations in Sections 1.3.2 and 1.3.3.

An assumption had to be made regarding the total length l of the dipole moment; this was rather arbitrarily set at 1 km. The electric moment was calculated to be 6.4×10^3 coulomb meters, and the following values of field strengths were then derived at a distance of 100 meters from ground zero;

H_ϕ = 515 ampere turns per meter

$E_\theta = 5.78 \times 10^7$ volts/meter

$\frac{dH_\phi}{dt} = 4.78 \times 10^7$ ampere turns per meter per second

The predominant frequency in the dipole current, i.e., at ground zero, was calculated to lie between 5 and 6 kc, showing that, as expected, lower frequency components have a relatively larger importance in the near-field region. Figure 1.1 shows the reconstructed pulse shape of the magnetic field as expected for a similar shot in the region of interest, and Figure 1.2 shows its derivative, which represents the voltage induced in a loop antenna.

1.3.6 Effect of Distance on Spectrum. The shifting of the Fourier spectrum of the pulse toward lower frequencies as the point of measurement is moved from the far (radiation) toward the near (induction and quasi-static field) regions can be shown by the following analysis.

Assume an ideal oscillating electric dipole in free space and let it radiate a pulse composed of many frequencies whose currents are in the same phase at zero time and distance. Consider two frequency components of the pulse, ω_1 and ω_2 (where $\omega = 2\pi f$), with corresponding transverse electric fields E_1 and E_2, and dipole moments M_1 and M_2. The problem is to predict how the amplitudes of the electric fields associated with the two frequencies vary with radial distance from the axis of the dipole.

In general, the transverse electric field component is given by:

$$E_\theta = \frac{MK^3}{4\pi\epsilon_0} e^{i(\omega t - Kr)} \sin\theta \left[-\frac{1}{Kr} + \frac{i}{(Kr)^2} + \frac{1}{(Kr)^3} \right] \tag{1.9}$$

Where: $K = 2\pi/\lambda$ = propagation constant
M = dipole moment
r = radial distance from the dipole

Let the two frequencies be related through the propagation constants by some ratio, $K_1 = AK_2$, where A is greater than 1. Let the dipole moments be in some other ratio, $M_1 = BM_2$, where B may assume any value. Using Equation 1.9, the ratio of the magnitudes of the two fields, $|E_1/E_2|$, for equal θ at any distance r, can be derived in terms of the constants A, B, and the distance r.

Taking the absolute value of E_1/E_2 and substituting for K_1 and M_1, the equation for the ratio of the fields at any distance r is

$$\left|\frac{E_1}{E_2}\right| = B \left[\frac{A^4(K_2r)^4 - A^2(K_2r)^2 + 1}{(K_2r)^4 - (K_2r)^2 + 1} \right]^{1/2} \tag{1.10}$$

In the vicinity of $r = 0$, the ratio $|E_1/E_2|$ is equal to B (the ratio of the dipole moments). At relative large distances (on the order of about a wavelength of the low-frequency component), the ratio is approximately equal to BA^2.

By differentiating $|E_1/E_2|$ with respect to r, and setting the derivative equal to zero,

$$(1 - A^2)\, rA^2 (K_2r)^4 - 2(A^2 + 1)(K_2r)^2 + 1 = 0 \tag{1.11}$$

Hence, for $A > 1$, the extrema occur at $r = 0$ (where $|E_1/E_2| = B$) and at the zeros of $[A^2(K_2r)^4 - 2(A^2 + 1)(K_2r)^2 + 1]$. Thus, a curve of E_1/E_2 versus rK_2 contains both a maximum and a minimum, which occur when

$$rK_2 = \left[\frac{(A^2 + 1) \pm \sqrt{(A^2 + 1)^2 - A^2}}{A^2} \right]^{1/2} \tag{1.12}$$

From Equation 1.10, when $A = 1$ (or $\omega_1 = \omega_2$), there are no maxima or minima, and the curve is a straight line. As A increases indefinitely, the position of the maximum approaches $rK_2 = \sqrt{2}$, or $r = \sqrt{2}\,\lambda_2/2\pi$. Figure 1.3 shows the general shape of the curve for $|E_1/E_2|$ versus rK_2 if B is held constant and A is varied.

On some of these curves a point may occur where $|E_1| = |E_2|$ (depending on the values of A and B). This point occurs at a distance

$$rK_2 = \left[\frac{(1 - A^2B^2) \pm \sqrt{(4B^2 + 4B^2A^4) - (3A^4B^4 + 2A^2B^2 + 3)}}{2(1 - B^2A^4)} \right]^{1/2} \tag{1.13}$$

For $|E_1| = |E_2|$ the following condition must be satisfied:

$$-3A^4B^4 + (4 + 4A^4 - 2A^2)B^2 - 3 \geq 0$$

From this condition it is found (by letting $A \to \infty$) that, if M_1 is larger than $2\sqrt{3}/3\ M_2$, the two fields can never be equal, no matter what value A is given.

Thus:

(1) Unless the frequencies are equal, the curve of $|E_1/E_2|$ versus rK_2 will always have a maximum and a minimum point whose positions depend only on the ratio of the frequencies.

(2) If M_1 is greater than $(2/3)\sqrt{3}\ M_2$, then the field associated with the higher frequency will always be greater than that of the lower frequency. If M_1 is less than M_2, the amplitude of the higher frequency field will be less than the amplitude of the lower frequency field at short distances. This is evident from the curve for $|E_1/E_2|$ versus rK_2.

(3) A low-frequency component that contributes relatively little to the radiation field cannot be ignored in the near field.

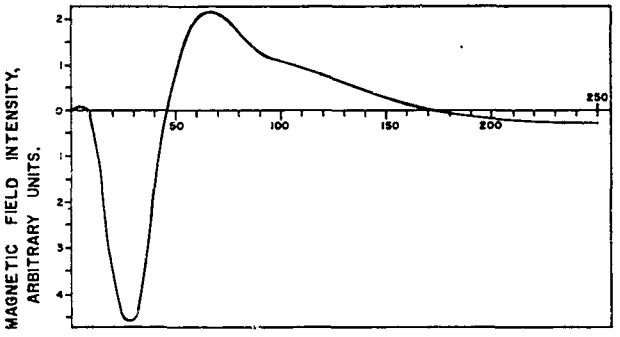

Figure 1.1 Predicted magnetic field intensity versus time (from zero time), microseconds.

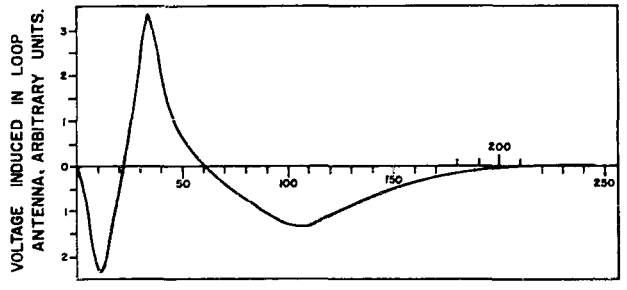

Figure 1.2 Predicted derivative of magnetic field intensity versus time (from zero time), microseconds.

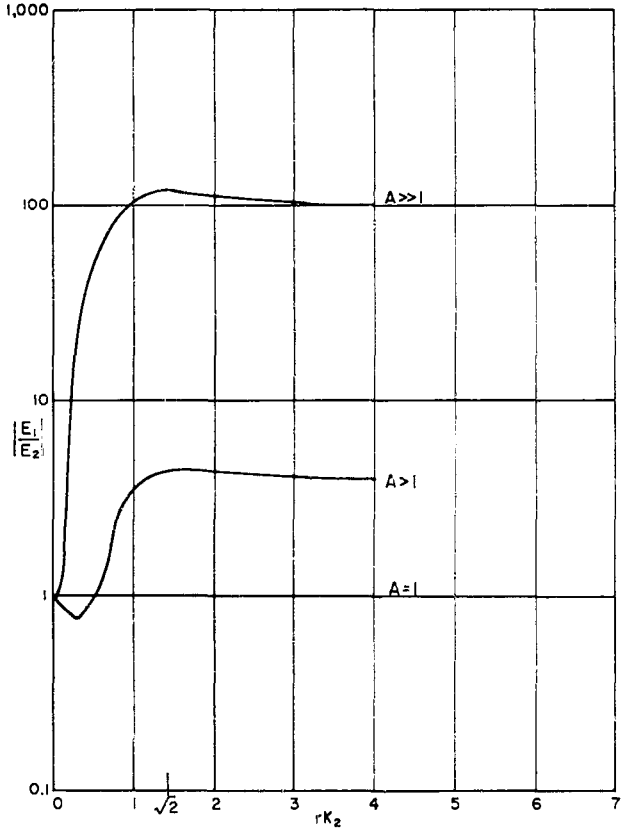

Figure 1.3 Ratio of field intensities versus distance frequency.

Chapter 2

PROCEDURE

2.1 RECORDING EQUIPMENT

From the calculations of the expected magnetic field intensity, it was estimated that the values of interest at the closest-in station (Station 1) would be somewhat between 1 and 20 oersteds. Five recorder stations were to be located at increasing distances from ground zero to a maximum distance of 16 times (Station 5) the closest-in station distance from ground zero. Assuming a peak signal of 10 oersteds at Station 1 and the worst possible predicted degradation of signal as the third power of distance, this would require a sensitivity of about 2.5 millioersteds with attenuators (with sufficiently variable steps) to a maximum of 72 decibels. The actual design sensitivity of the instrumentation that could be reached without an excessive requirement on power, noise, etc., was 10 millioersteds full-scale at maximum gain with a dynamic range of about 30 decibels. If the peak signal strength were 10 oersteds at about 5 kc at Station 1, this design would make it possible to record the same signal level at all stations by setting the gain to the maximum at Station 5 and introducing sufficient attenuation to record full scale at Station 1.

The expected signal had strong frequency components in the 1- to 30-kc region for most weapons. Occasionally, fairly strong components have been noted up to 50 kc, and rarely has anything of comparable field strength been noted above 100 kc. Since a loop antenna yields a voltage that is the time derivative of the magnetic field, signal components should extend up to 200 kc, at most. The major requirements were, therefore, for an instrument with a large dynamic range, broad frequency coverage, and excellent shielding against direct pickup, i.e., other than through the antenna. These specifications were met by a self-contained, low-input impedance, wide-band, rugged magnetic tape recorder.

The instrument was designed to have the following characteristics:

(1) Its total recording time had to be sufficiently long to have stabilized by shot time (assuming it had been previously turned on by a timing signal) and to allow recording through the arrival of the blast wave. This period was dictated by an estimate that some very-low-frequency components (below 100 cps) noted on at least two previous occasions were connected with the shock wave.

(2) The recorder had to be completely self-powered, since power lines, signal lines, or both, could serve as source antennas to introduce unwanted signals into the electronics.

(3) Integrating circuitry was required to obtain the desired record of magnetic-field changes versus time, since the voltage across a low-impedance loop antenna is proportional to the time derivative of the magnetic field. Integration can be performed before recording by suitable electronic circuits, or after playback by electronic or graphical means. Neither method appeared entirely satisfactory alone; thus, for reliability, a dual-capability was provided for recording both the differential signal and the integral of a loop antenna output. For an additional freedom of choice, the integrating circuit could be bypassed to permit a straight-recording of the antenna output.

(4) The recorder had to be capable of simultaneously recording the signals from preferably three and at least two differently oriented antennas, since the actual spatial direction of the magnetic field at the close-in distances could only be surmised but not definitely predicted.

(5) It had to be capable of withstanding and recording through the accelerating forces caused by the passing shock wave at the closest-in station. At this point the acceleration was estimated

not to exceed 50 g in any direction.

(6) It had to be electromagnetically shielded sufficiently well so that the very large electric field could not bypass the antenna and become impressed directly on any portion of the recording circuitry.

(7) Since the magnitude of the expected magnetic field was only calculated, for safety purposes the instrumentation had to be capable of recording full-scale values at least 10 times higher than those expected, i.e., up to 100 oersteds at frequencies of about 5 kc.

2.1.1 System Design. The final design of the instrumentation system consisted of signal pickup loops, shielded signal lines, and a shielded package containing a magnetic tape recorder, together with associated electronics control circuits and power supplies (Figure 2.1).

The more desirable system, which would place the instrumentation at a safe distance from the detonation, was ruled out, since the enormous electromagnetic field would make impossible the use of long signal lines.

Consequently, the system was completely self-contained and required only two timing signals—one at t_0 (detonation time) minus 5 minutes to turn on the equipment early enough to provide adequate tube warmup and circuit stabilization, and a second signal to start the tape recorder at t_0 minus 60 seconds so that the recorder would be up to speed at t_0 (Table 2.1). These control signals were to be furnished by Edgerton, Germeshausen and Grier, Inc. (EG&G), which had sole responsibility for generating and distributing the timing signals to the nuclear weapons and all the instrumentation.

Automatic circuits disconnected the recording systems from the timing lines after the second timing signal and then shorted them to preclude the possibility of their serving as antennas that would inject large signals through the package shielding.

The system package requirements were dictated by the severe environment to which it would be subjected during its recording cycle. Since the close-in instrumentation installation would be virtually in the fireball of the detonation, mechanical and electronic design requirements were severe. The instrumentation not only had to live through the detonation and perform its normal recording function but also was not to be influenced by any of the detonation forces except those that acted on its input transducers. Moreover, only low-cross-section, short half-life materials could be used throughout so that test personnel could recover the equipment without undue delay. The difficulty of the problem was not mitigated by the fact that the magnitudes of these forces were arrived at by calculation and extrapolation from incomplete previous data.

To protect the system from the considerable ground shock and nuclear radiation near ground zero, the recorder package was hung on springs from heavy timbers 12 feet underground in a concrete-lined hole. Electrically shielded cables led upward from the recorder to the information-sensing loops, which were mounted at, or slightly below, the surface of the ground. Sandbags were piled on top of the recorder for shielding from nuclear radiation, and a massive wooden structure supported the weight of the sandbags.

These precautions were intended to protect the equipment from overpressure loading and ground shock. The long slant distance through the earth from the point of detonation of an airburst provided considerable neutron and gamma shielding. Magnetic shielding, which attenuates the introduction of a signal at any point except at the input loops, was an integral part of the recorder package. The magnetic shielding problem requirements were severe for the recorder package, since it contained high-gain electronics in addition to sensitive magnetic recording heads.

2.1.2 Magnetic Shielding. The recording system was inclosed in a 0.125-inch-thick Armco iron box with a hermetically sealed cover, which served the function of the outer magnetic shield and a mechanical housing.

The degree of shielding required was based upon (1) the predicted maximum field of 10^6 volts/meter, (2) a 1-meter maximum length of conductor within the shield, and (3) the lowest signal

that conventional electronics can readily detect, or 1×10^{-5} volt, i.e., an attenuation factor of 10^{11} was required (neglecting reflection from the shield surface).

The iron box was chosen for the outer magnetic shield to preclude the possibility of saturation in the very high field. The attenuation factor of this shield section (again neglecting reflection) was calculated to be 4.5×10^{-5}, which would reduce the field to a value where the more efficient Mu-metal could be used.

Two mutually insulated 0.025-inch-thick Mu-metal shields were placed inside the outer iron shield.

The effectiveness of the combined triple-shield was calculated by use of the skin depth expression (assuming 1,000 cps to be the lowest frequency component to be shielded)

$$H_i \text{ (or } E_i) = H_0 \text{ (or } E_0)\, e^{-x/\delta}$$

Where: $\delta = \sqrt{\frac{2}{\omega\mu\sigma}}$ meters

$\mu = \mu_{rel}\mu_0$

$\omega = 2\pi f$

$= 2\pi 10^3$ cps

σ = conductivity (mho/m)

$\mu_0 = 4\pi \times 10^{-7}$ henry/meter

The following very conservative assumptions were made:

$$\mu_{\text{Armco iron}} = 200\mu_0$$

$$\mu_{\text{Mu-metal}} = 10^4\mu_0$$

$$\sigma_{\text{Armco iron}} = 10^7$$

$$\sigma_{\text{Mu-metal}} = 2 \times 10^6$$

Therefore, the composite shield composed of one thickness of 0.125-inch iron and two thicknesses of 0.025-inch Mu-metal will attenuate a signal by:

$$4.5 \times 10^{-5} \times 6.25 \times 10^{-6} = 2.8 \times 10^{-10}$$

Although this might seem marginal, it must be remembered that this figure is based on the effect of the field on a 1-meter length of wire and neglects any field reduction by reflection. In the actual recorder, all signal leads were kept well below this value, and most of these leads were shielded, twisted pairs a few inches long.

The two Mu-metal shields were insulated from each other by a 0.125-inch layer of felt (Figure 2.1), which served to provide high resistivity between shields, protected the relatively sensitive Mu-metal from shocks that might change its magnetic characteristics, and provided a considerable degree of thermal shielding.

2.1.3 Antenna System. Each antenna consisted of six turns of polyethylene-insulated No. 18 copper wire wound inside of a split toroidal copper shield. The mechanical arrangement can be seen in Figure 2.1. Two antennas were oriented 90° apart so that two components of the electromagnetic field could be recorded simultaneously on two channels. One of the loop antennas used is shown in Figure 2.2. The lines that fed the signal from the pickup loop antennas to the instrumentation package required extremely effective shielding. Unlike the leads inside the recorder package, which could be held to a few inches in length, these had to be over 3 meters long and to carry signals of 10 volts or less through fields of perhaps 10^6 volts/meter to high-gain amplifier inputs. Such leads could, as open wires, have spurious emf's as high as 4×10^6 volts induced on them.

Two precautions calculated to preclude this possibility were taken:

(1) A balanced line within the triple-shielded coaxial cable was used to feed the signal to the

recorder package. Any induced voltage would be introduced in each side of the line in phase and of equal amplitude; whereas the input circuit at the recorder input required equal signal voltage 180° out of phase. The system was balanced so that in-phase rejection of induced signal voltages was in excess of 60 decibels.

(2) The coaxial shields were connected only at the loop antenna (single point grounding), and each shield was connected to its associated shield in the recording system shield box, i.e., the outer shield was connected to the outer iron box, the next inner shield connected to the next inner Mu-metal shield, etc. The coaxial shields were composed of flexible, armored cable similar to electrical BX, which gave a relatively high shielding factor. The shielded signal lines were fed into the electronics through attenuators, which could be preset to any value from 0 to 80 decibels, according to the expected field strength.

2.1.4 Recording System. The system had a basic recording capability of seven analog HF bias-type channels on 1-inch magnetic tape.

Although it would have been desirable to record over a continuous frequency range from several cycles per second to several hundred kilocycles, this was impracticable at the then-existing state of the magnetic tape art.

Analog AM recording can be successfully accomplished over a frequency range of about 20 to 1. Since the upper frequency limit set by head design, tape transport speed (120 in/sec), and length of recording was about 200 kc, the lower limit became about 1,000 cps. Slightly lower frequencies can be recorded but at a cost of increased low-frequency distortion, loss of dynamic range, or both.

A subcarrier-type FM recording system is quite the reverse, however, since it is capable of recording data from dc up to a frequency determined by carrier frequency, deviation, allowable distortions, dynamic range, and subcarrier bandwidth requirements. Moreover, since the FM system utilizes discrete carrier frequencies, several channels may be multiplexed on a single recording track. Therefore, two separate systems, one amplitude modulated and the other frequency modulated, were developed. The former covered the range from 300 cps to 200 kc, the latter from somewhat slightly below 1 cps to 5 kc. The crossover point was at 3 kc, with 12 decibels per octave dropoff on both sides. Two separate carrier frequencies, 36 kc and 120 kc, were used in duplex for the FM system, yielding four available channels for the low-frequency band on two recording tracks (of the available seven), while four more tracks were used in the AM system for the higher frequency band.

The remaining recorder track was reserved for timing signals. Two signals were provided: (1) a fiducial marker to accurately establish time zero and (2) a continuous sinusoidal signal to establish accurate time intervals after t_0. The center track on the tape was reserved for these timing signals, since the other tracks would be symmetrically disposed about it and thus halve the azimuthal alinement errors.

Because prompt gamma radiation would reach the recording position in a fraction of a microsecond, it was used to establish t_0 by arranging a pulse generator circuit utilizing a gas tube, which would conduct when ionized by the arrival of gammas and cause a high-amplitude pulse to be recorded on the timing channel. The 10-kc timing signal, generated by a stable plug-in vacuum tube oscillator circuit, was recorded on the timing channel.

Selector switches allowed the operator to choose the recording of either the derivative of the magnetic-field change or its integral on each channel. The input signal could also be simultaneously connected to two channels through different attenuators. This was especially helpful in the early stages of the experiment, providing an expanded scale required because of the uncertainty of the expected signal input values. Since the recorder itself provided a dynamic range of about 30 decibels up to 100 kc, a setting of, for instance, 0 decibel on one and 20 decibels on other attenuator resulted in a usable range of 50 decibels.

All the preceding circuitry, including a second antenna, was duplicated in the other half of the recorder, making a total of two complete broadband combined integrated and nonintegrated channels available.

A block diagram of the system can be seen in Figure 2.3.

2.1.5 Magnetic Heads. A survey of the magnetic tape recording art and commercial practice made it clear that a research and development program had to be instituted to extend the commercially available magnetic recording bandwidth by a factor of 2.5. Discussions with leading recording engineers confirmed the opinion of DOFL engineers that the state of the magnetic head art at that time was the bandwidth limiting factor.

At the same time, the Naval Ordnance Laboratory (NOL) published a report describing a new magnetic material developed by that laboratory, which was composed of (the nonstrategic materials) iron and aluminum. This alloy was called Alfenol.

NOL had compiled considerable data on the use of Alfenol for relatively low frequency magnetic tape head applications (0 to 45 kc) but had virtually no experience with its characteristics at the higher frequencies. Since NOL was anxious to gain data on applications of Alfenol, a sample quantity of magnetic head lamination stock from Alfenol 16, rolled to 4-mil thickness, was provided to DOFL for this experiment.

DOFL undertook to produce a workable magnetic recording head model capable of response to over 200 kc at a reasonable tape transport speed. The first problem to be solved was that of designing and fabricating a magnetic recording head capable of recording frequencies of about 200 kc. Consideration of the interrelated problems of head wear, bandwidth, and tape deterioration versus speed characteristics suggested that 120 in/sec was the highest reasonable tape speed. This fact, then, set the basic requirements for the recording head design. The design of a recording head using Alfenol was not a straightforward problem, since there was no design data available on this material.

Two 7-channel head assemblies were built, using the best of the contemporary techniques. The units were identical except for the use of Alfenol laminations in one unit (Permalloy was used in the other unit). There was neither time nor design data available to optimize either unit to establish an absolute comparison. The Mu-metal head could not be operated at the 500-kc bias frequency without excessive head power requirements (due to core losses), which precluded optimum operation without introducing the possibility of serious heating and possible damage such as gap spreading. The Alfenol head, however, worked satisfactorily with 500-kc bias and power requirements within reasonable limits (Figure 2.4).

There are a great number of interrelated factors that have to be considered in the design of a multichannel record head, such as core material, inductance, gap, cross-talk, frequency response, Q, and mechanical configuration.

A toroidal configuration with balanced windings offers a number of advantages (the most important of which is its immunity to external magnetic fields) essential for use in the detonation environment. The absolute gap dimension is not critical as long as the back edge of the gap is straight and reasonably continuous. The conventional way to lap the head pole faces to optical tolerances is to split the toroidal core and lap the faces. This method requires the use of a spacer in the back gap, which is of identical dimension to the front gap. Although the back-gap type of recording head exhibits a lower efficiency and requires higher values of signal and bias current, it is relatively less sensitive to variations in inductance, which makes possible the holding of track-to-track inductance variations within very close tolerances.

The Q of such a head with a 1-mil gap is less than 2.0. If a head is prepared without the back gap, the efficiency can be as much as 20 decibels higher with a Q as high as 3, but the inductance spread even with close winding control can vary 2 to 1, or more. Since input signal data was scant at the time the heads were developed for this project, the low-Q design was decided upon to insure very high uniformity between channels, which would help insure consistent, correlatable data. Moreover, since the magnitudes of the input signals were estimated, it was deemed wise to use magnetic head designs that did not saturate easily.

Head design problems could be segregated into two categories. The requirements were for (1) a record head that would handle the required bandwidth with low distortion and adequate signal-to-noise ratio, and (2) a reproduce head capable of reproducing the signals recorded by the record head. The reproduce head was needed to evaluate the record system both in the development laboratory and to read out data in the field. The problems presented are different because of the basic difference in operation of the two systems. The flux in the record head

and hence the magnetic field strength across the tape is proportional to the current in the record head. The reproduce head output voltage, however, is dependent on the rate of change of flux produced by the magnetic poles recorded on the tape as they move past the reproduce head (and thus on the tape speed).

Since the mechanism of magnetic recording involves only the trailing edge of the record head, the gap dimension does not determine bandwidth. The trailing edge of the record head must be straight and smooth, since even small irregularities cause field concentrations (of bias) sufficiently great to erase the higher signal frequencies after they have been recorded.

The record head must have sufficiently high inductance to be easily driven by conventional electronics, yet low enough to resonate at or above the bias frequency, here, 500 kc. The efficiency of the head must be great enough to operate at optimum bias levels without overheating. Since the bias level is about 10 times the signal level, heating problems become increasingly serious as the bias frequency is raised. Ideally, the frequency chosen for the bias should be no less than five times the highest signals superimposed upon the recorded signals. All of these problems are intensified since this system required seven tracks to be mounted in one assembly with a 40-decibel or better interchannel crosstalk requirement. Moreover, the gap scatter had to be held to less than one gap width to maintain the absolute time integrity of the pulse information on the tape.

Reproduce head inductance should be as high as possible to produce maximum output voltage subject to the requirement that the head resonance falls well above the highest signal frequency (250 kc).

2.1.6 HF/AC Bias Requirement Determination. An analog magnetic recording system requires an HF/ac bias to be mixed with the intelligence signal to maintain very low distortion by maintaining the recording medium in the center of the linear portions of its hysteresis loop.

The suitability of an Alfenol head could not be completely assessed until the proper bias requirements were established. Bias requirements vary greatly, depending upon the absolute values of such parameters as core material, inductance, gap, track width, signal bandwidth, tape type, transport speed, bias frequency, and allowable distortion. Instrumentation required to perform the bias requirement determination comprise a magnetic tape reproduce system of known characteristics. This system included a suitable tape transport mechanism, a reproduce head with known response characteristics, a reproduce amplifier with known characteristics including a bandwidth in excess of that to be measured, and distortion low enough to be considered negligible (0.1 percent of lower), as well as a suitable vacuum tube millivoltmeter and an oscilloscope. In addition, a record amplifier was required capable of driving the record head with a constant current versus frequency characteristic over its entire frequency range. This determination consisted primarily of running a family of frequency response curves over the required bandwidth (1 to 250 kc).

The effect of varying the HF bias is to cause the signal HF sensitivity to change inversely with LF distortion. A compromise had to be effected between acceptable distortion at the lowest signal frequency and the maximum acceptable attenuation of the highest signal frequency.

In general, at the higher signal frequencies, a high value of bias tends to erase the recorded frequencies, while at the lowest signal frequencies the hysteresis loop operating characteristics of the magnetic core material require higher values of bias. The bias requirements must be determined for the specific type of magnetic tape that is most suitable for the recording job to be done. Other tapes are not interchangeable with the chosen tape without adjustment and recalibration of the bias record system.

The bias is usually obtained from a stable, low-distortion power oscillator. Amplitude stability is important, because the intelligence HF amplitude and LF distortion are a direct function of bias amplitude. Variations in bias amplitude of ± 1 decibel are considered the limiting acceptable value for all changes due to components and supply voltages.

Even more important—very good waveform symmetry must be maintained. Output waveform asymmetry will appear as a dc component in the record head, which will displace the zero signal operating point from the center of the hysteresis loop characteristic with an

attendant reduction in dynamic range, and increased noise and distortion.

Small variations in bias oscillator frequency, per se, are of secondary importance except where it (1) affects output amplitude or waveform or (2) varies outside the frequency limits of bias traps on isolation circuits in the record or reproduce amplifiers.

In multichannel record systems, the bias signal for each record head must be isolated from each other head to eliminate signal crosstalk. It is usually not feasible to use separate bias oscillators for each channel, since it is nearly impossible to shield the channels well enough to preclude beats between the bias oscillators. Separate oscillators can be used, however, if they all operate at the same frequency, by introducing synchronizing signals between them. A great reduction in circuit complexity was effected by using one bias oscillator and an isolation amplifier stage between it and each record head. In addition to reduced circuit complexity, the following advantages accrued from this choice: (1) the bias oscillator did not have to supply the bias power, resulting in improved stability and waveform; and (2) bias adjustment of each channel did not affect the oscillator.

The bias oscillator signal amplitude was about 10 times the intelligence signal amplitude. Care had to be exercised to prevent the former from leaking into the signal circuits where it could influence the operation of these circuits in addition to generating beat signals. This is particularly important when the bias signal frequency approaches the higher signal frequencies. As stated earlier, the minimum design rule of thumb dictates a bias frequency at least five times the higher signal frequency. In this record system, this was impossible because of head core limitations, so effective bias rejection filters had to be interposed between the record amplifiers and each record head.

2.1.7 Tape Transport. The function of a tape transport is to cause magnetic tape to be transferred at a constant rate from one reel to another, passing over magnetic recording heads on the way. All design efforts are pointed toward insuring constant tape speed and constant intimate contact between the magnetic surface of the tape and the activated area of the recording head. Even partial accomplishment of these goals requires the maintenance of extreme rigidity between mechanical members, usually necessitating a heavy cast "plate" upon which the mechanical components are mounted. Sometimes an even more rigid assembly is required, which may take the form of a box-shaped aluminum casting. Such a machine is manufactured by the Cook Electric Company. This recorder, used by DOFL in this project, operated at a tape speed of 120 in/sec and included provision for mounting a 7-channel magnetic record head. This transport (Cook Electric MR 315) originally designed for use in rocket sleds for the U. S. Air Force, was capable of operating during 50-g accelerations. It included an armored, takeup-reel housing to protect the tape record even in the event of severe tape puller damage. The machine provided capacity of 1-inch-wide, 1.5-mil-thick tape sufficient for a total recording time of 45 seconds (at 120 in/sec).

The Cook tape transport was powered by a 24-volt dc "synchronous" motor containing a vitrating-reed-type speed-regulator system capable of holding speed variations, wow, and flutter to values approximately equivalent to an ac hysteresis synchronous motor powered from the usual 110-volt, 60-cps power line.

The transport was modified by DOFL engineers to include a head pad to insure contact between the record head and the tape, and to include a recorder timer, which took over the various switching functions of the entire recorder from 60 seconds before until 45 seconds after detonation.

With the sequence timer geared directly to the transport drive, an absolute timing relationship was maintained between the switching functions and the actual position of the recorded signal on the tape. This latter feature was desirable, since the total available recording time was only 45 seconds and since about 20 seconds of this was used to accelerate the tape to 120 in/sec and 20 seconds for recording the field signal. An error of several seconds in timing might have caused the desired signal to be recorded during tape acceleration, destroying the frequency accuracy of the record. Shortening the 20-second recording time would cause loss of information on possible long-persistence field strength variations. The modifications

performed by DOFL engineers on the Cook tape transport can be seen in Figures 2.5 and 2.6.

2.1.8 Electronics. The electronics were packaged into individual plug-in modules (Figure 2.7) and included the following: preamplifiers and integrator circuits, multiplex circuits and timing oscillator, and recording electronics.

In the interest of extreme flexibility, the recording system was designed to accept input signals over a range of about 100 decibels. This was accomplished by providing high- and low-gain plug-in preamplifier modules in addition to adjustable input attenuators.

To record H as well as dH/dt, an integrator circuit was provided, which could be connected between the antenna and the recorder. Two plug-in integrator units (Figures 2.8 and 2.9) were required per channel. One was designed to perform its integration functions over the HF band and the other over the LF band. The integration characteristics were obtained through balanced reactive feedback loops.

Two channels of LF information were FM multiplexed on one track at two carrier frequencies selected to produce a minimum of interaction while maintaining adequate bandwidth.

DOFL-designed FM modulator units (Figures 2.10 through 2.12) were packaged in the form of plug-in modules, which simplified field service problems and reduced the possibility of obsolescence for future test programs.

The multiplex FM modulators were designed to operate at subcarrier frequencies of 35 and 110 kc, respectively. The circuit used in both the LF and HF modulators was an adaptation of the phantastron oscillator, cathode modulated by the varying R_p of a modulator triode.

This circuit (Figures 2.10 through 2.12) could be deviated ± 20 percent with less than 1 percent total harmonic distortion, with an input of 300 mv.

The timing osillator unit (Figure 2.13) contained a subminiature pentode RC oscillator followed by a subminiature triode cathode follower.

Since the RC oscillator design was relatively insensitive to variation in supply voltages and the effects of the nuclear environment, it was not necessary to provide a balanced output (Figure 2.13). The signals from the attenuators had to be amplified by relatively high gain, balanced preamplifiers with a high in-phase rejection ratio before they could be fed to either the modulators or the record amplifiers (in the case of HF channels) (Figures 2.14 through 2.16).

The recording electronics, also packaged as plug-in modules consisted of: record amplifiers, bias oscillators, and bias isolation amplifiers.

The record amplifier was required to transform a small transducer output voltage into a current sufficiently great to drive the record head. The head driving stage had to provide a constant current versus frequency characteristic over the range from 1 to 250 kc with a dynamic range of over 35 decibels.

The bias oscillator had to provide a stable output voltage at 500 kc with very pure waveform. In particular, the waveform had to be symmetrical, since any asymmetry resulting in a dc component in the head circuit would degrade its signal-to-noise ratio and LF response.

Isolation means (usually amplifiers) were required to prevent crosstalk between channels, since the bias connections to each head would effectively place all of them in parallel, and to reduce the power requirements on the oscillator, which would result from connecting seven head circuits in parallel to the oscillator output circuit. Considerable oscillator power was required to develop sufficient bias current in the head (approximately 10 times the signal current or 10 ma per head).

The record electronics had to be miniaturized to fit in a reasonable-sized package, ruggedized to withstand very severe physical environment and be arranged in a plug-in configuration to facilitate field servicing and to allow rapid change in the system as required for the different phases of the tests. Complete interchangeability of all of the components in the record system package (plug-ins, heads, etc.) made it possible to use five machines interchangeably, both within one test and from test to test, and resulted in saving of time sufficient to allow field personnel to include additional tests to answer questions that arose as data from each test was processed.

The record amplifier (Figure 2.17) was designed to supply an essentially constant current signal to the record head over a frequency range from 60 to 330,000 cps. It consisted of a push-pull RC-coupled power pentode amplifier stage utilizing two miniature 5686 tubes. The relatively low impedance output circuit was fed to the heads through a series resistor and a pair of bias trap coils, which prevented the relatively high amplitude bias signal from feeding into the record amplifier plate circuit and modulating the information signal. The series-resonant bias trap coils consisted of miniaturized 465-kc ferrite core radio IF coils, which could be tuned exactly to the 500-kc bias frequency and had sufficiently high Q to exceed the design requirements of 40-decibel attenuation.

The pentode design was used for several reasons, the more important of which included, in addition to the higher power sensitivity, taking advantage of the constant current characteristic of a pentode to drive a load (the head) that requires a constant current signal. Also, a pentode is relatively insensitive to the actual value of load resistance in that its distortion does not increase rapidly as the plate load impedance is lowered below its plate impedance as a triode does.

The bias oscillator (Figure 2.17) design comprised a push-pull tuned plate type with balanced capacitive grid plate feedback. The tank coil consisted of the primary winding of a ferrite cup core transformer the secondary of which fed a push-pull resistance-coupled triode amplifier stage with RC plate-grid negative feedback, which served the dual purpose of providing a low-impedance driving voltage to drive the seven bias isolation amplifiers and isolating the oscillator from the loading of the seven bias circuits. An adjustable common cathode resistor was provided to balance the amplifier circuit to reduce the distortion to the practical minimum. Since distortion-measuring equipment that would operate at 500 kc was unobtainable at the time, direct distortion measurements could not be made.

Signal distortion measurements were made, however, at the low signal frequencies; these were considered an adequate indication of bias distortion, since bias level considerations are based in part on the LF distortion, which varies inversely with frequency. The total distortion due to bias waveform asymmetry and record amplifier distortion measured at the lowest signal frequency (1,000 cps) was less than the value considered acceptable for recording the data (3 percent).

A balanced push-pull amplifier (Figure 2.17) was interposed between the bias oscillator and the record head for each track of the record system. This amplifier, utilizing two power pentode 6005 miniature tubes, not only supplied the head circuit with the proper bias current but also provided adequate isolation between the head and the record amplifier and more than adequate isolation between tracks.

This circuit complication, additional space, and power drain were justified, since the disadvantages were more than outweighed by the following: (1) lowered power requirements for the oscillator, which would otherwise be greater than could be supplied with miniature tubes; (2) optimum impedance match to the head, which would preclude loading of the record amplifier output circuit; (3) individual adjustment for optimum bias for each track without interaction on the other track; (4) over 40-decibel reduction of the track-to-track crosstalk, which is a serious problem in a common bias system; and (5) considerable reductions of noise modulation and distortion due to the reaction of the bias signal on the plate circuit of the record amplifier. (A filter was inserted in the record amplifier plate circuit to further reduce this effect.) Without the bias amplifier, this filter would have been very complex, which would have degraded the good system transient response.

The bias signal was fed from the bias amplifier to the head via a balanced output transformer and blocking capacitors.

The record system, including the record electronics, bias oscillator, bias amplifiers, and heads, utilized completely balanced circuitry, which effected maximum rejection of electromagnetic signals necessary in near-field measurements.

2.1.9 Power Supply. The instrumentation required a self-contained recording system, which dictated the use of battery power as a primary power source. Early planning resulted in the

decision to use a single battery of secondary cells, mainly because the expected extensive development, test, and service time of primary (or dry) cell batteries would require too much space, cost too much, and have questionable reliability when subjected to all of the aspects of a nuclear detonation.

A study of the problem revealed that the best compromise in the selection of secondary cell batteries was the hermetically sealed nickel-cadmium Voltabloc battery. This 28-volt, 35-ampere unit was exceedingly rugged, was capable of withstanding many charging cycles, was able to deliver large currents in a short period of time, and was possessed of a flat discharge versus voltage characteristic.

2.1.10 Recorder Package. The recorder inner package occupied a volume of 8 cubic feet arranged in a cube with 24-inch sides. The outer frame of 2-inch aluminum angle stock was welded into two box sections, which could be swung apart on a piano hinge for ease in servicing. When swung together, the two sections, alined with guide pins, were held together with heavy bolts. Two lifting rings were attached on a vertical line through the package center of gravity. All of the sides were flush so that the package could be easily slid into the outer magnetic shield assembly. Flexible cable connections ran between the sections so that it would operate in a normal manner with the sections swung apart. All of the electronics were located in the smaller of the two sections and the timing, power, and tape transport mechanisms in the other.

The various components can be seen and identified in Figures 2.18 through 2.21. Notice that every component is accessible for adjustment or replacement, in spite of the staunch frame.

The tape transport was located in the top of the power section of the recorder package so that the magnetic tape could be removed and replaced without removing the recorder package from the outer magnetic shield.

Because of the considerable weight of the recorder package, servicing facilities were set up in the field with benches arranged in a quonset hut in such a way that a small crane could lift the recorder assembly from the outer magnetic shield while outside the hut, swing the package into the hut, and deposit it in the servicing position. The photographs in Figures 2.22 through 2.24 show the recorder being placed in the outer magnetic shield box and the complete system being installed into the container well of the site.

2.2 CALIBRATION

Calibration was performed before installation of the station and after recovery; a complete tape with sufficient amplitude and frequency characteristics was recorded both times and retained for future evaluation and signal analysis.

The simplicity of the loop antenna operating below its self-resonant frequency permitted an easy calculation of the value of the time derivative of the magnetic field, since:

$$(\text{induced voltage}) = -NA\,\mu_0 \frac{dH}{dt}, \tag{2.1}$$

Where: N = number of turns
A = area of loop, m^2

Since the characteristics of the integrators were known, the value of the magnetic field could be calculated. Pre- and postshot calibration tapes were analyzed in the laboratory and, together with the known electronic integrator characteristics, were used to prepare the sensitivity data, in ampere turns per meter or ampere turns per meter per second, for each recording channel at each station and recorder.

2.3 METHOD OF INSTALLATION AND RECOVERY

The recorder boxes had to be protected from the effects of overpressure, and although the tape puller was capable of operating under high acceleration, it was desirable to reduce the shock to a minimum by suitable shock mounts. Furthermore, the electronics had to be pro-

tected from appreciable nuclear radiation, since at the high radiation intensities present at and immediately past time zero, induced transient currents and, at the closest distance, even permanent degradation would result.

Subsurface installations were, therefore, planned. Calculations were made to determine the depths necessary for reduction of neutron dosage to 10^8 neutrons/cm^2 and gamma dosage to 0.3 r for the largest shot in which each station participated. The deepest hole measured approximately 9 feet to the surface of the recorder shield, whereas the outermost stations measured 1.5 feet. To accommodate the instrumentation boxes, all holes were 5 feet square.

For best results, the entire space above the instrumentation should have been filled with soil; this, however, would have introduced a serious recovery problem. Sandbags grouped in standard Army cargo nets were used as the cover instead, and care was taken not to leave large voids through which neutron leakage could occur. The recorder box was suspended by four springs (resonant frequency approximately 2.5 cps, maximum excursion 3 inches) mounted to an aluminum hanger plate bolted to lumber hangers that fitted into concrete slots. A cover of 4- by 10-inch lumber (maximum dimensions for the deepest hole) rested on a concrete lip and served to support the sandbags and protect the recorder from the overpressure. The transmission and timing lines fitted through slots in this cover and extended up to the loop antennas, which were buried 1 to 2 feet below the surface. The attenuation of the signal through the amount of soil covering the antennas was negligible at the frequencies considered. Unreinforced concrete was used as a liner, because the introduction of conducting materials, such as steel in a reinforced structure, would seriously distort the electromagnetic signal.

2.4 STATION LOCATIONS

Figure 2.25 and Table 2.2 give the location of each station and the slant range to each shot.

2.5 DATA REQUIREMENTS AND ANALYSIS

Information was required on the amplitude of the magnetic field component of the electromagnetic field as a function of time. The recovered magnetic recording tapes for each shot were played back at the instrument truck at Camp Mercury, and the data obtained was used as guidance to set the unit attenuators for succeeding shots.

The signals on the recording tapes were displayed on an oscilloscope and photographed. Those pictures showing no overload characteristics were then used for scaling purposes. By means of the calibration tapes and their accompanying oscillograms, the output voltage from the playback amplifier was related to the input voltage to the recorder. The information of primary interest obtained in this manner was the peak field intensity, the peak value of its time derivative, and, in some cases, the time to the first peak and the crossover.

A more complete analysis was performed at DOFL. The interim test report stated that no LF channels could be played back at Mercury because of excessive noise as well as frequency and voltage variations in the power supplies for the playback equipment. Under the more favorable laboratory conditions, it was possible to extract the LF data. A great deal of this turned out to be overloaded, since no attenuator setting corrections could be made in the field because of the playback problem at that time. Sufficient data was obtained, however, to yield a fairly good estimate of the general character of the signal.

TABLE 2.1 RECORDER EVENT SEQUENCE

EG&G EXTERNAL SIGNAL	INTERNAL MAIN TIMER (MIN)	RECORD TIMER (SEC)	MAIN TIMER DIAL READINGS	FUNCTION	POWER DEMAND VOLTAGE (V)	POWER DEMAND CURRENT (AMPS)
T_0 -5 min.			1	TIMING MOTOR STARTS	27.0	0
	-4.5		2	TIMING CIRCUITS ON	27.0	4.0
	-3.5		3	FILAMENTS ON	26.0	14.6
	-2.5		4	INVERTER ON	25.5	30.8
	-1.5					
T_0 -1 min.		-60	5	RECORDER TIMER ON	25.3	30.6
		-55		RECORDER TIMER LOCKED ON		
	-0.5					
		-20		TAPE TRANSPORT STARTS	25.0	34.6
	0.0		6	EXTERNAL TIMING LINE DISCONNECTED		
T_0 DETONATION		+20		TAPE TRANSPORT STOPS	25.0	30.5
	+0.5			INVERTER OFF		
		+45	7	RECORDER TIMER OFF	25.0	15.0
	+1.5		8	FILAMENTS OFF	26.0	3.5
	+2.5		9	TIMING MOTOR STOPS	26 +	0

TABLE 2.2 SLANT RANGES OF STATIONS

Only stations from which data was collected are listed.

Station	Shot	Slant Range from Burst Zero meters
Frenchman Flat		
F6.2-9037.03	Priscilla	938
F6.2-9037.04	Priscilla	2,200
Yucca Flat		
9-6.2-9006.01	Hood	498
9-6.2-9006.01	Lassen, Wilson, Owens	250
9-6.2-9006.02	Hood	566
9-6.2-9006.02	Lassen, Wilson, Owens	368
9-6.2-9006.03	Hood	887
9-6.2-9006.03	Lassen, Wilson, Owens	776
9-6.2-9006.04	Hood	1,590
9-6.2-9006.04	Lassen, Wilson, Owens	1,532
9-6.2-9006.05	Hood	2,930
9-6.2-9006.05	Lassen, Wilson, Owens	2,901
2A-6.2-9001	Diablo	298

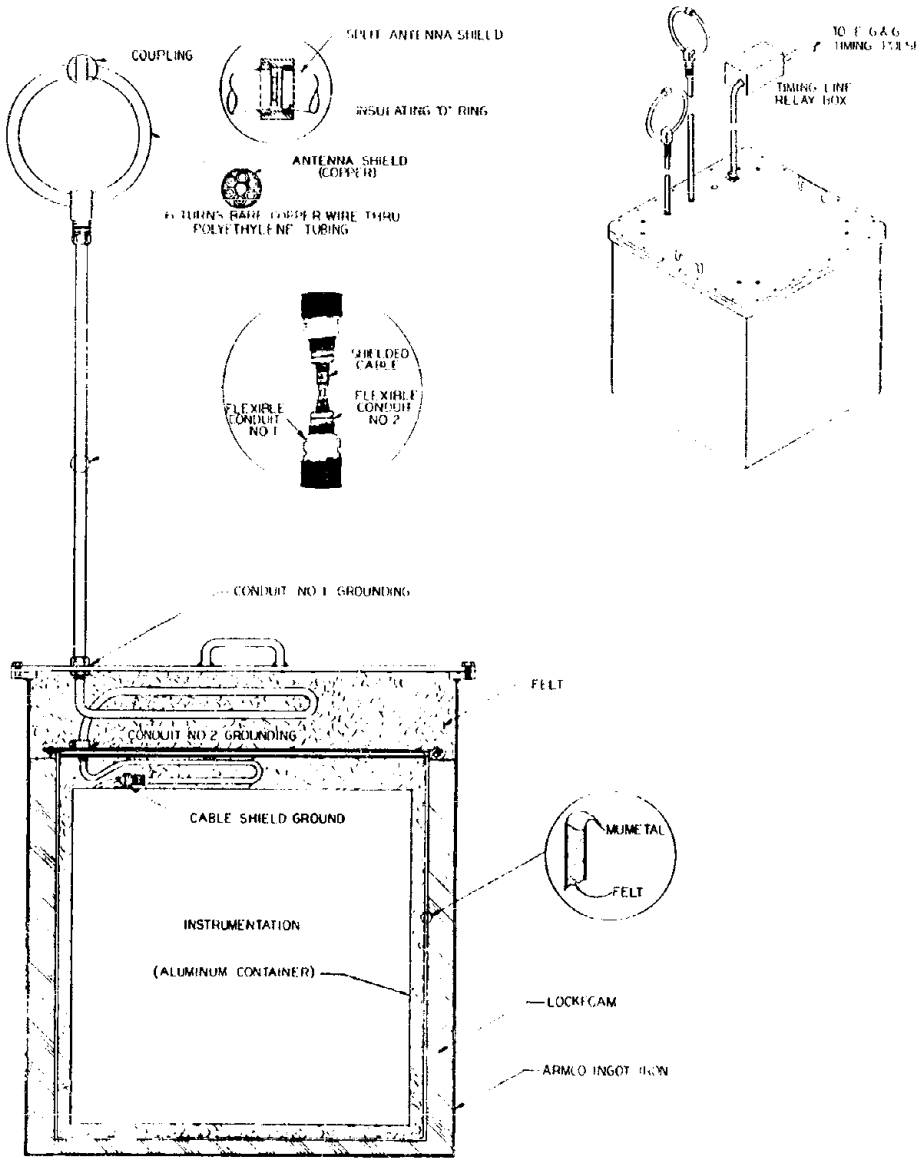

Figure 2.1 Instrumentation system package.

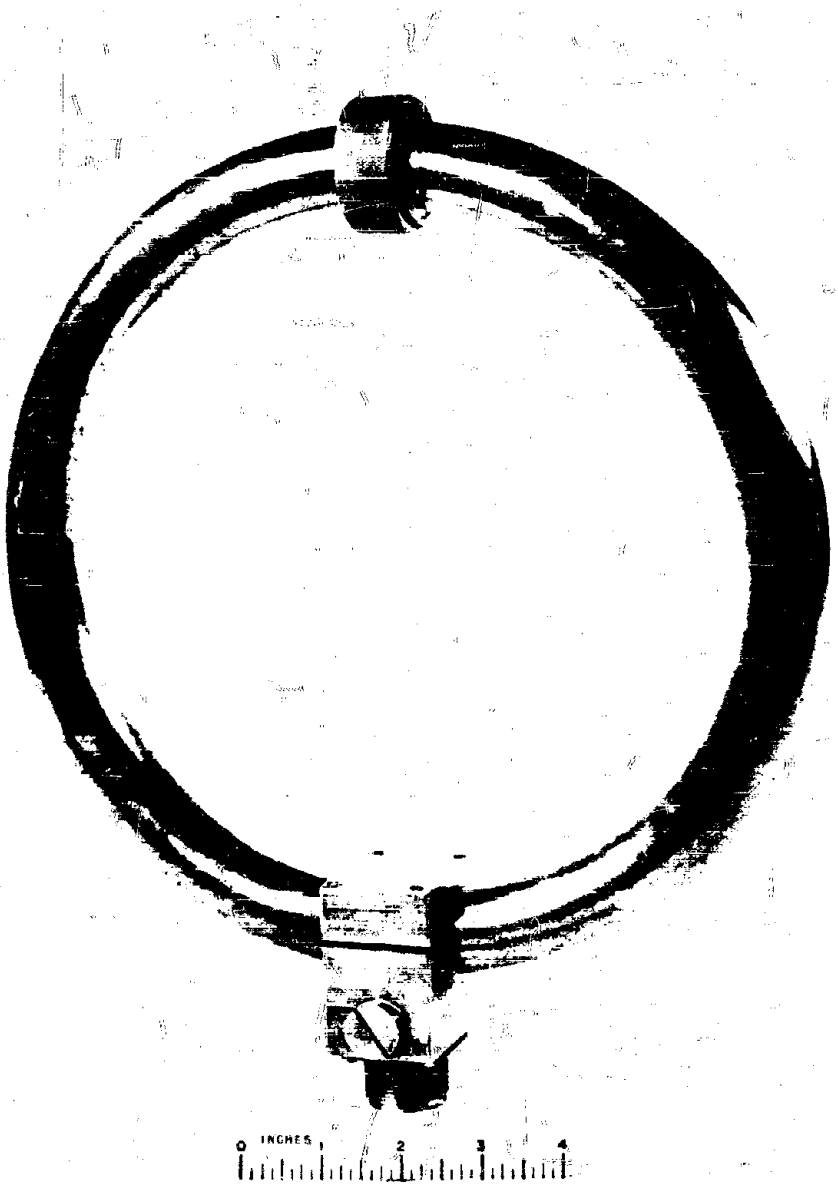

Figure 2.2 Loop antenna.

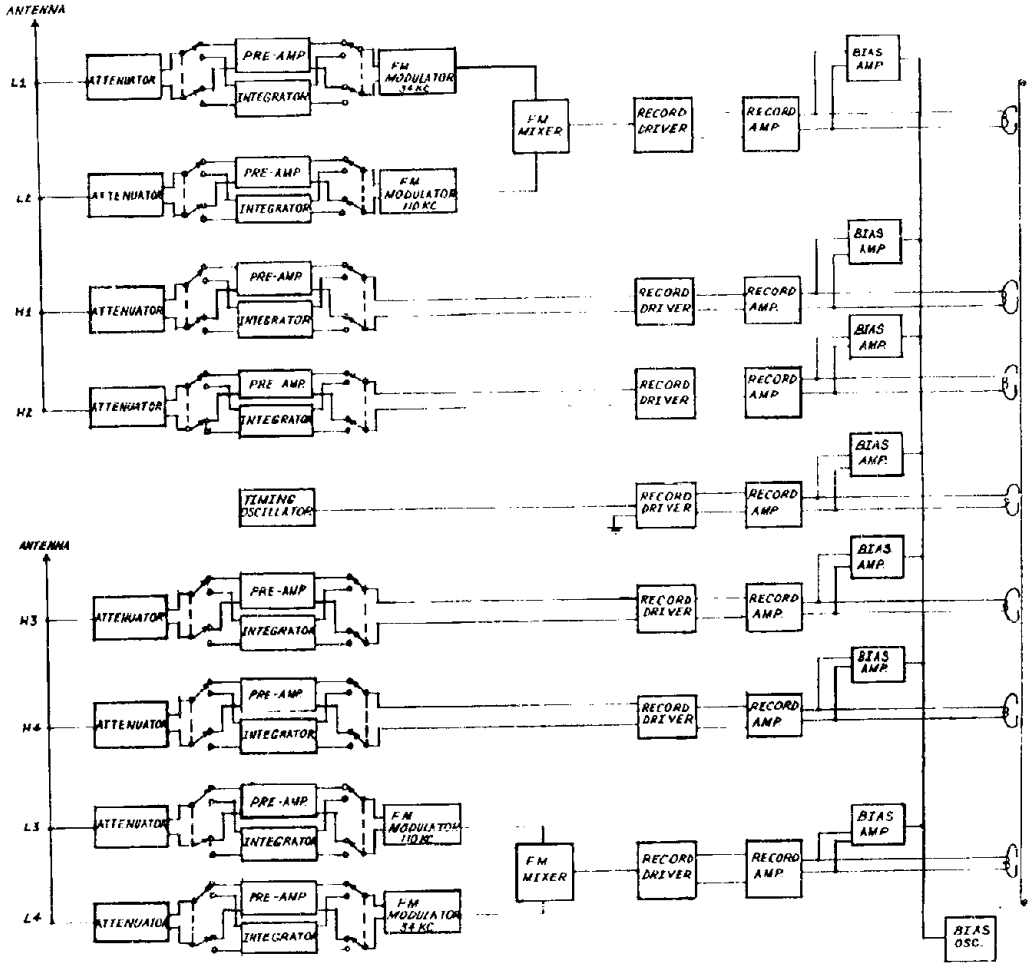

Figure 2.3 Block diagram of instrumentation system.

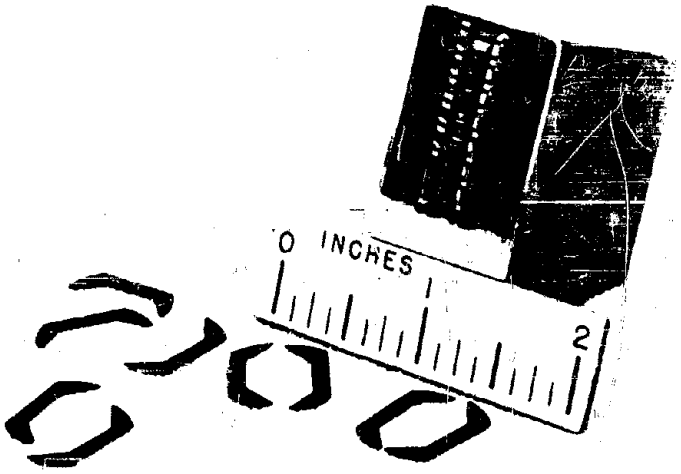

Figure 2.4 7-channel magnetic head.

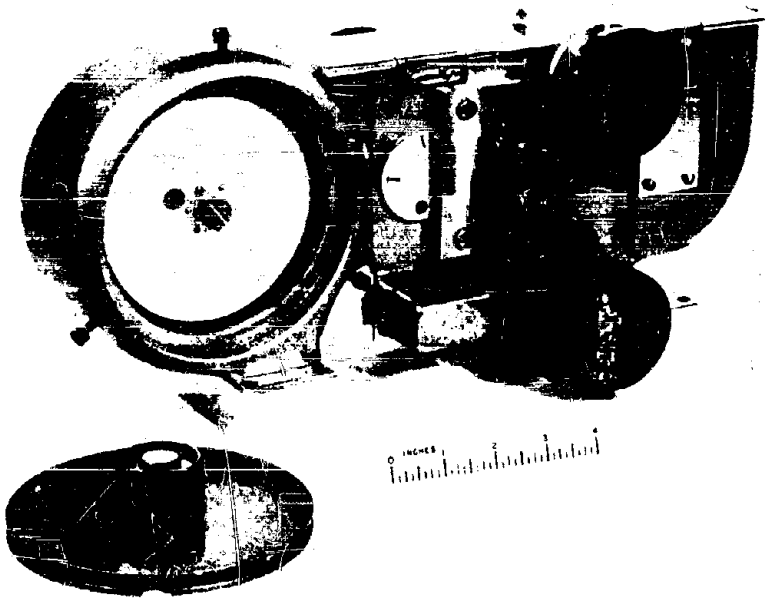

Figure 2.5 View of tape transport, showing armored tape compartment and timer.

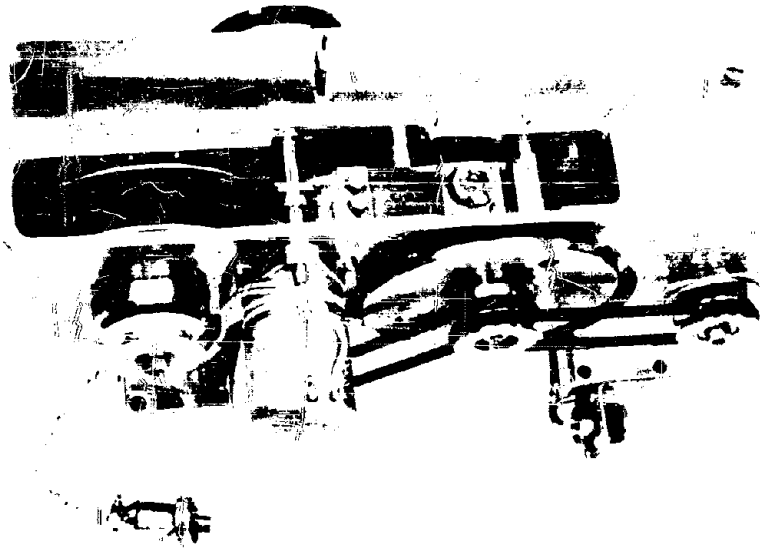

Figure 2.6 Top view of tape transport, showing tape path.

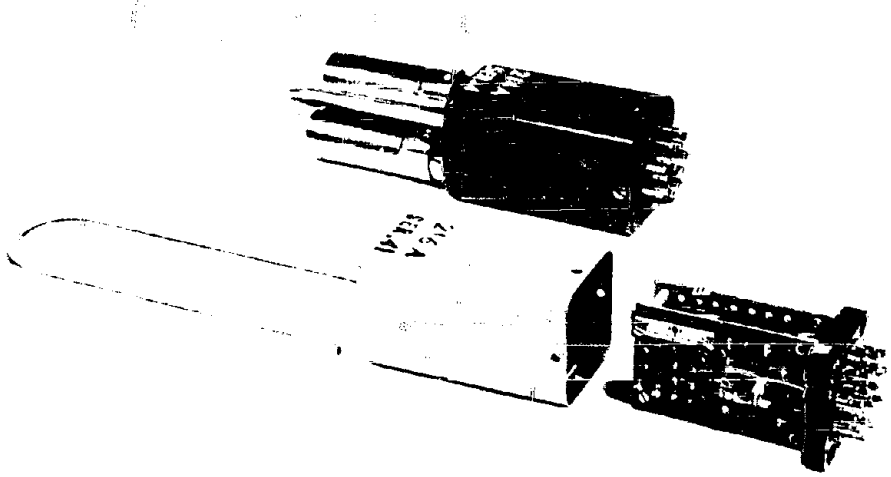

Figure 2.7 Tape recorder plug-in units.

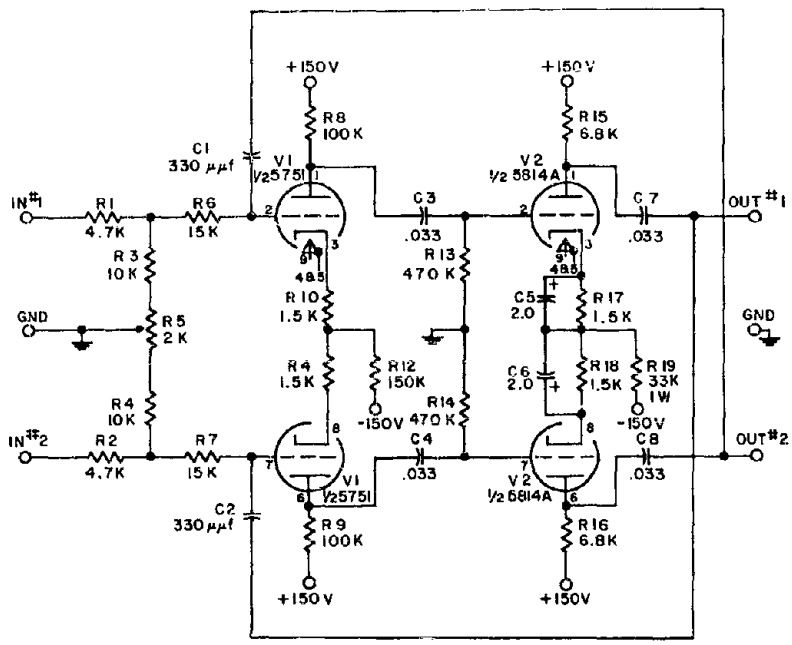

Figure 2.8 Schematic of high-band integrator.

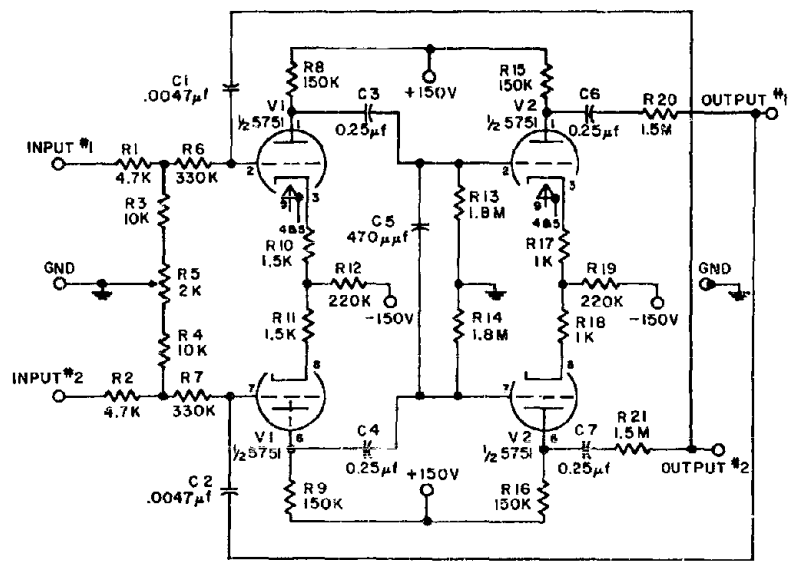

Figure 2.9 Schematic of low-band integrator.

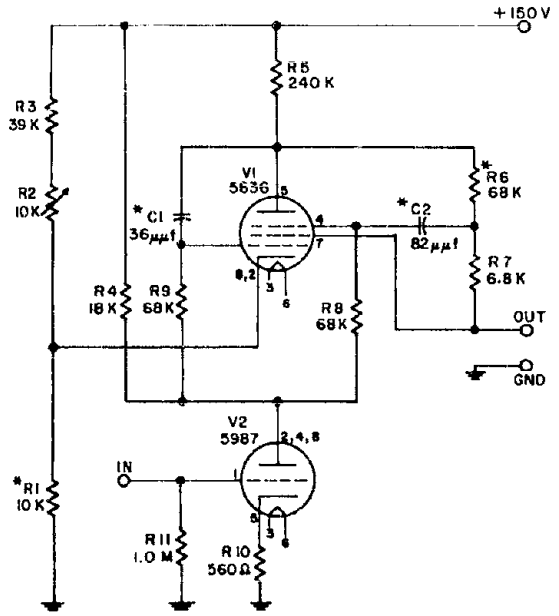

Figure 2.10 Schematic of FM modulator, HF band.

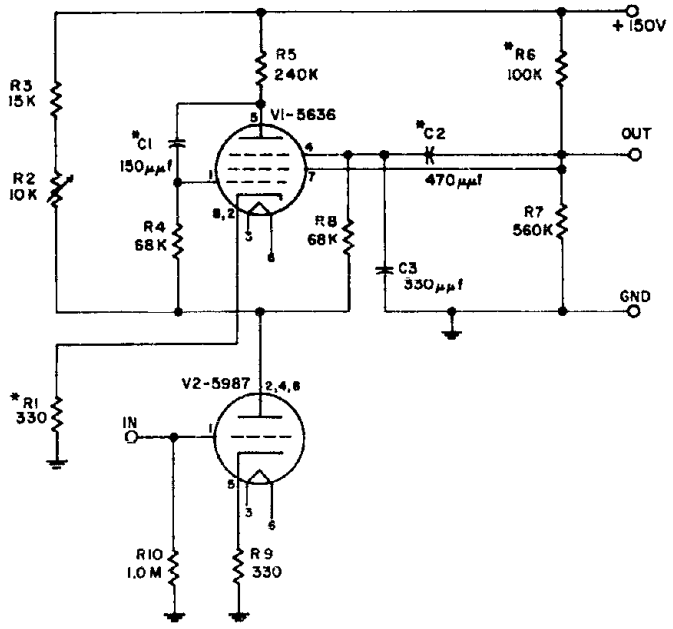

Figure 2.11 Schematic of FM modulator, LF band.

SECRET

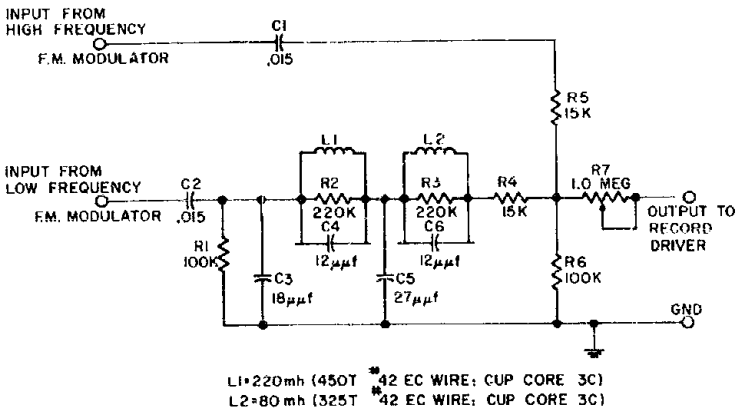

Figure 2.12 Schematic of mixer filter.

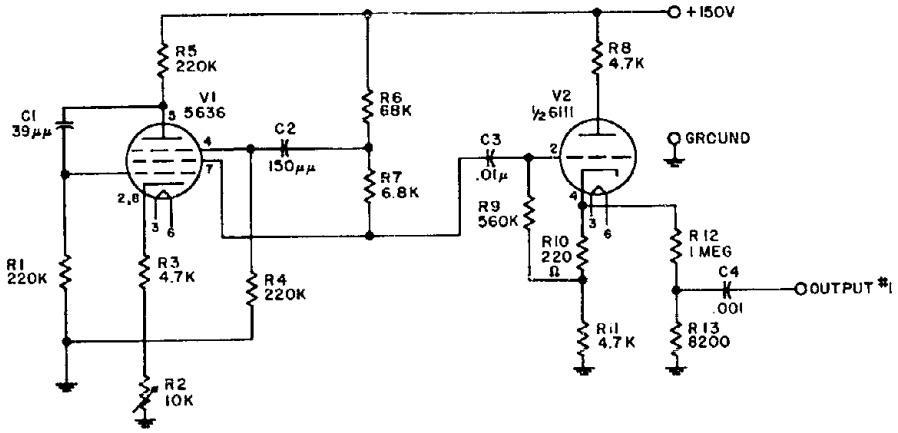

Figure 2.13 Schematic of timing oscillator and cathode follower.

SECRET

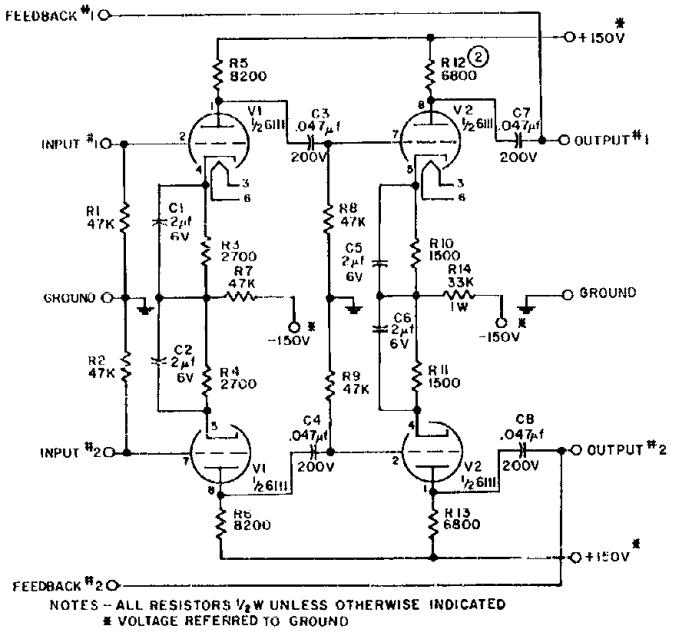

Figure 2.14 Schematic of high-band preamplifier 1.

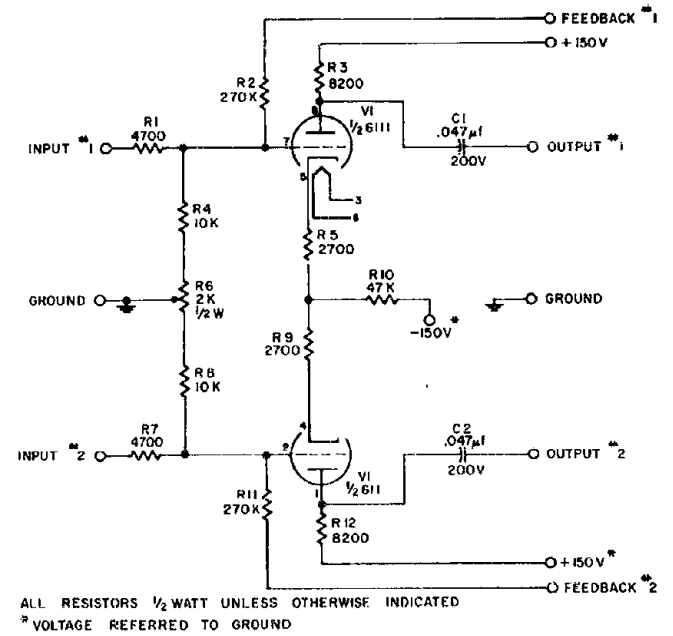

Figure 2.15 Schematic of high-band preamplifier 2.

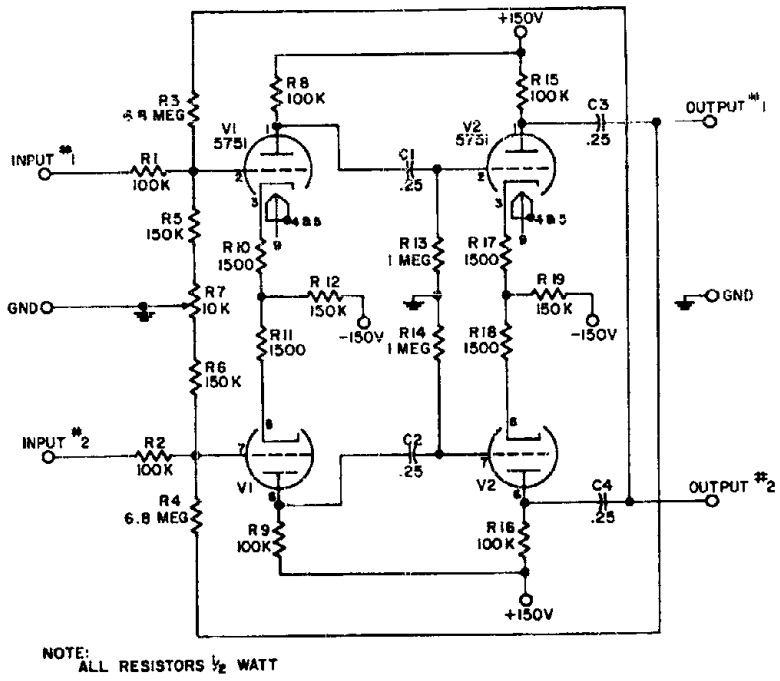

Figure 2.16 Schematic of low-band preamplifier.

SECRET

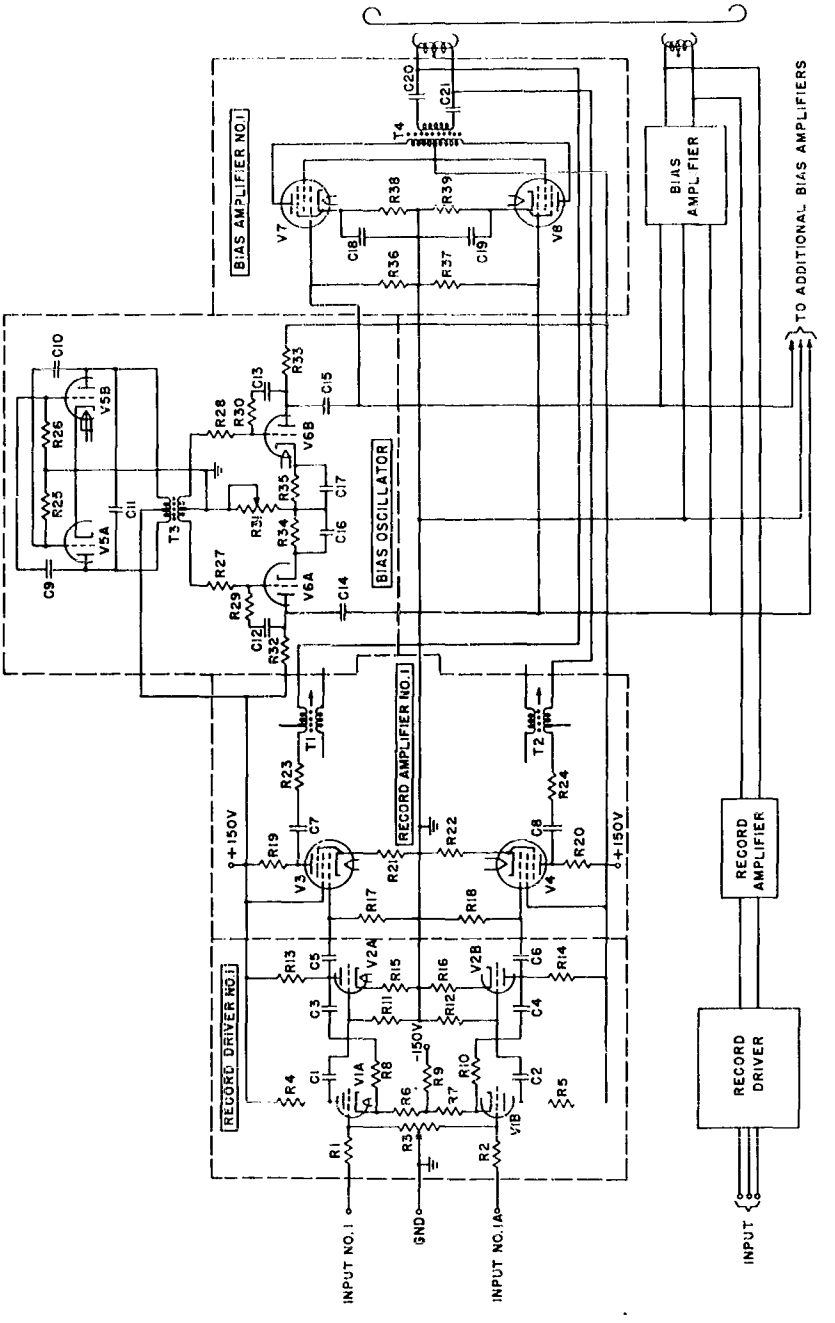

Figure 2.17 Schematic of recorder electronics.

SECRET

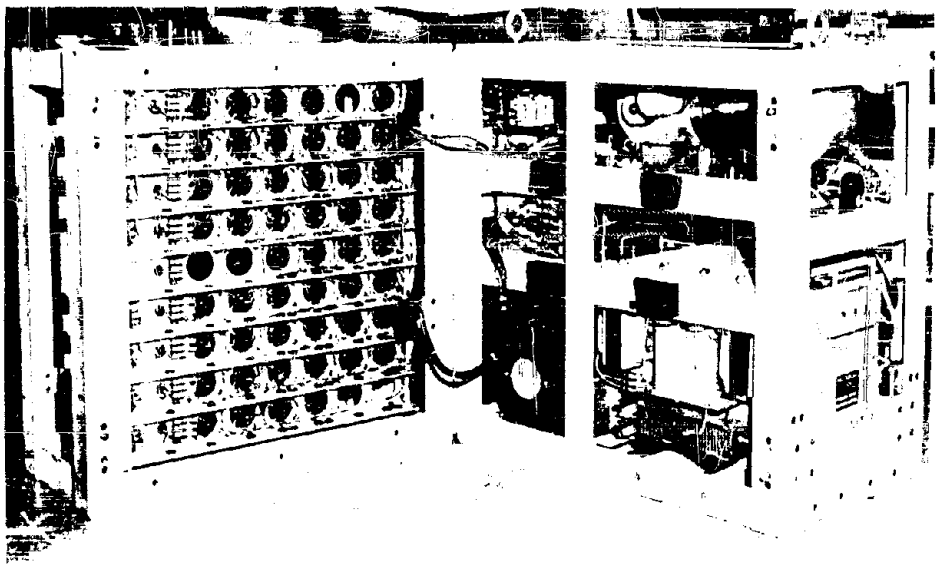

Figure 2.18 Recorder, inside view.

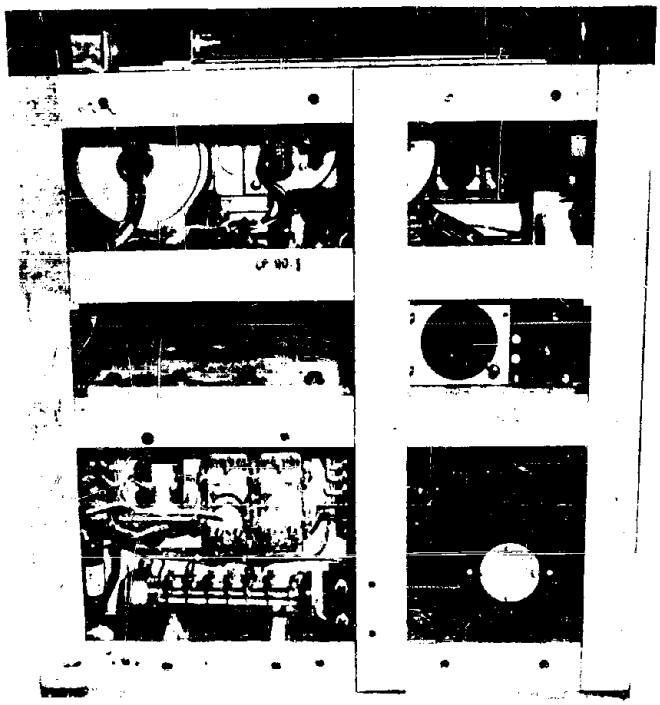

Figure 2.19 Recorder, end view.

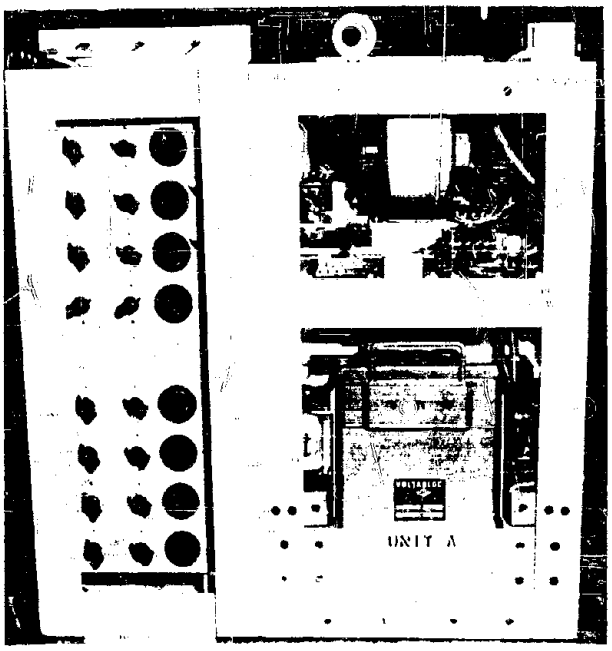

Figure 2.20 Recorder, side view.

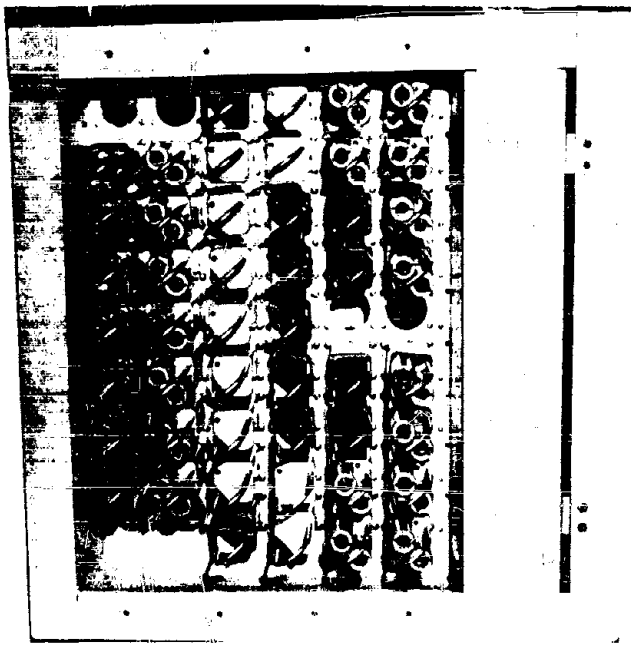

Figure 2.21 Recorder, side view.

Figure 2.22 Recorder package being transferred from service area to outer magnetic shield box.

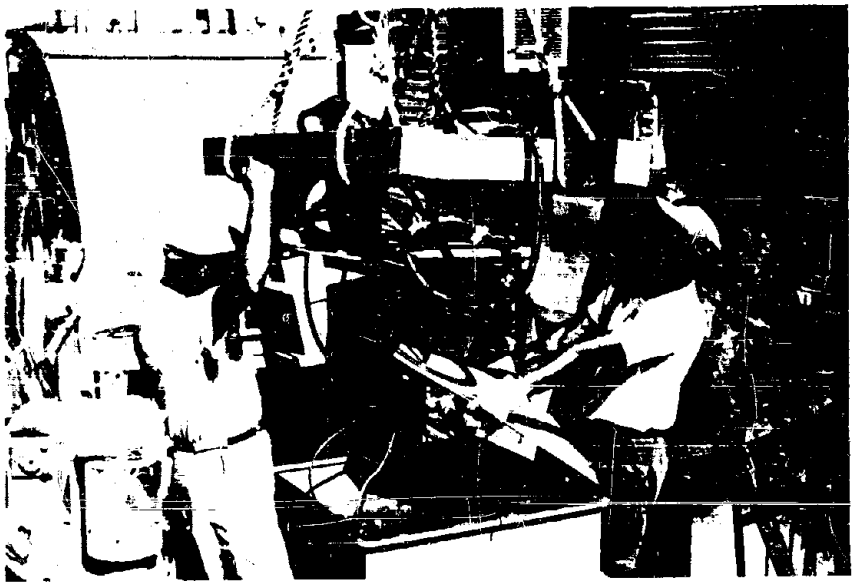

Figure 2.23 Lowering recorder package into magnetic shield box.

Figure 2.24 Lowering recording package into hole.

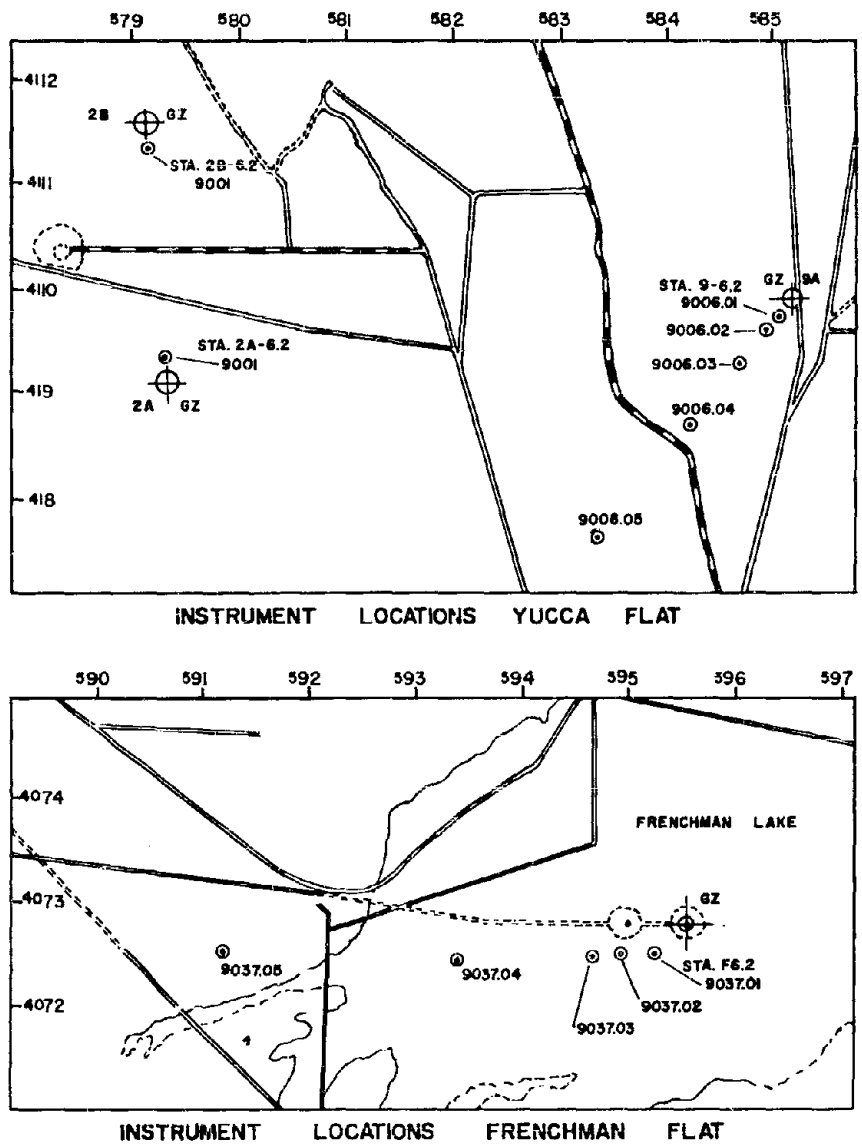

Figure 2.25 Station locations.

Chapter 3

RESULTS

3.1 DEGREE OF SUCCESSFUL PARTICIPATION

The project participated in six shots: Lassen (0.47×10^{-3} kt), Wilson (10.3 kt), Priscilla (36.6 kt), Hood (71 kt), Diablo (17.0 kt), and Owens (9.7 kt). Useful data was obtained on each of these events.

3.1.1 Shot Lassen. Although the yield of Shot Lassen was considerably below that expected, data was obtained at two stations. Regardless of the low yield, the peak values of dH/dt were only two orders of magnitude below those of some of the later shots with yields of from four to five orders of magnitude higher.

3.1.2 Shot Wilson. It had been hoped to use the data from Shot Lassen to estimate the values for Shot Wilson, but because of Lassen's low yield, this was not advisable. The project, therefore, instrumented for Shot Wilson identically to Lassen, and obtained records at all five stations. This was essentially the project's first participation and, therefore, the data obtained was somewhat scant.

3.1.3 Shot Priscilla. Instrumentation for Shot Priscilla consisted of five recorders. Amplitudes were predicted by using the Wilson data and a relation involving the square root of the yield ratio, as suggested by staff members of LASL. Good data was obtained at Stations 3 and 4. The sensitivity setting for Station 5 turned out to be too low; thus, no data was obtained at this station. The first and the project's only recorder failure occurred at Station 2 as a result of the omission of a recorder drive belt before installation. The project had participated in several successful timing runs before D−1 day and had noted no failures up to that date. On D−1 day, a timing signal distribution box, located some 25 feet from Station 1, was sandbagged by EG&G. The last timing run on D−1 was a hot run, and no personnel could be stationed on the site. Subsequent examination, in the afternoon of D−1 day, indicated a failure of the timing relays at Station 1. The Test Director was notified of this fact, the notification was acknowledged, but no corrective action was authorized. When Shot Priscilla was later postponed for 1 day, it was apparently still not possible to effect any correction of this failure. The recorder at Station 1, therefore, received no timing signal, resulting in complete loss of data.

3.1.4 Shot Hood. Five recorders were placed in Area 9 for this shot. Predictions for signal amplitudes obtained with data from the previous shots proved to be good. Usable records were obtained at all stations.

3.1.5 Shot Diablo. Two recorders were used during Shot Diablo. Nearly 60 tons of lead shielding entirely inclosed the device. The signal was expected to be considerably below those previously obtained; therefore, a wide range of attenuator settings was used to prepare for either the usual signal or a much-reduced signal. In spite of these precautions, no record could be found on any of the channels at the farther out station. A signal, of the same order of magnitude as that obtained in Shot Lassen, was recorded at Station 1.

3.1.6 Shot Owens. The project used three recorders. Predictions of the amplitudes to be

obtained at this shot, gathered from the previous shots, turned out to be most valuable in this case. Good data was recorded at each station on nearly every channel of recording.

3.2 DISCUSSION OF DATA

Tables 3.1 through 3.4 give summaries of the amplitudes of the first peak of the magnetic fields and their time derivatives. The slant-range distance to the burst zero is given for each shot since, as will be shown later, it appears this is the most meaningful quantity. In addition to the peak amplitudes, the peak amplitudes divided by the square root of the yield are given for H_ϕ and dH_ϕ/dt and the peak amplitudes divided by the yield to the 0.4 power are given for H_r and by yield to the 0.7 power for H_z and their time derivatives.

In many cases, overload signals resulted in no usable data on several channels. An extensive examination into the overload characteristics of the recorders used resulted in an ability to make estimates as to the minimum values that could have resulted in such overload signals. Where such estimates were possible, minimum values are stated in the tables accompanying the oscillograms in the next section.

Tables 3.1 through 3.4 are divided into data from the HF and LF channels. In each case, the peak amplitudes stated as recorded by LF channels occurred at times subsequent to those noted under the HF channel captions. In nearly all cases, however, they appear to be of the same orders of magnitude. A further discussion of this phenomenon appears in a later section.

An extensive examination has been conducted into the behavior of the integrators. It is concluded that the designs were quite successful, that integration was performed relatively faithfully, and that it is possible to approximate the peak time derivative value by dividing the peak integrated signal by its rise time.

3.3 PRESENTATION OF DATA

3.3.1 Introduction. Oscillograms of the recorded signals, both from the HF and LF channels are presented in Figures 3.1 through 3.7 and referenced in Tables 3.5 through 3.8. These tables show what data the project set out to collect during each shot and at what station. They, furthermore, reference the reader to the oscillograms pertaining to the data and denote minimum values estimated from overloaded channels.

A word needs to be said about the LF channels. The HF cutoff on these was about 5 kc; thus, some of the HF signals, successfully recorded on the HF channels, did get through the amplifiers and were recorded at a much lower rise time and with decay periods pertinent to that portion of the system. Experiments with the response of the LF channels to sharply rising signals leads to the conclusion that the first few hundred microseconds and perhaps even the first millisecond should be disregarded except as evidence of the existence of an early HF signal.

The LF integrators had decay times with an e-folding period of approximately 80 msec. Thus, an oscillogram taken from an LF integrated signal channel should be interpreted as follows:

(1) A trace rising to a peak in a fraction of a millisecond should be disregarded and assumed to be the LF response of a fast rising pulse. When available, the HF channel trace should be used instead for that portion of the time history.

(2) A trace rising to a peak in one or several milliseconds is a relatively faithful reproduction of a magnetic field strength with that rise time.

(3) The decay of the trace from such a peak to zero, if appreciably faster than 50 msec, is probably a faithful reproduction of field strength decay with that time constant; if of the order of 0.1 second or larger, it probably means that the field strength remained at or about its peak value for a period longer than that. In the latter case, or where doubt existed, oscillograms have been presented showing the field-time dependence only to its peak value.

3.3.2 General Description of Signals. As expected, the signals mostly had rise times of

the order of several microseconds. It is well understood that the very first part of the signal should indeed rise considerably faster, beyond the rise time of this recording equipment; however, at the short distances at which these measurements were performed, very little energy is contained in that time portion, and the fields continue to rise with time constants of microsecond order. This same result has been confirmed by the British (informal discussions with S.D. Abercrombie, Atomic Weapons Research Establishment, Aldermaston, Great Britain) who, using 30-Mc cutoff-frequency equipment, have made similar electric field measurements at comparable distances.

The magnitude, although not the existence, of the very-low-frequency signals were somewhat surprising. An examination of the oscillograms shows that probably two separate signal time histories are present, the long persistent one starting after termination of the short duration signal. These signals coalesce as the distance to burst is decreased. This latter phenomenon has also been observed by the British.

The magnitudes of the signals appear to be in generally good agreement with those predicted in Chapter 1. The existence of appreciable fields in the H_z and H_r orientation is not too surprising in view of the complex nature of the source.

3.4 ANALYSIS OF DATA

3.4.1 Introduction. Figures 3.8 through 3.11 show the relationship of the amplitudes of the first peaks of the magnetic fields and their time derivatives to the slant range to the burst point. It should be noted that a cylindrical coordinate has been used instead of the spherical one discussed in Chapter 1. Since all measurements were made in the ground plane ($\theta = \pi/2$ or $z = 0$), there exists only an artificial difference between these two systems (because an H_θ field in this plane is entirely in the z direction). In the right-handed cylindrical coordinate system used, positive fields indicate a radial (H_r) field pointing outward from a vertical line through the burst point, a vertical (H_z) field pointing upward and an azimuthal (H_ϕ) field pointing counterclockwise. Thus a positive H_ϕ is that as would eminate from current flowing upward. The amplitudes have been normalized by dividing the actual values by the yield raised to some power n as indicated in Tables 3.1 through 3.4.

3.4.2 Scaling Laws. To establish scaling laws for the magnetic field with yield Y and distance R, the following relation was assumed.

$$H = \frac{K\ Y^n}{R^m} \tag{3.1}$$

Taking the logarithm of both sides yields

$$lnH = lnK + n lnY + m lnR \tag{3.2}$$

This has the form

$$Y = a_0 + a_1 x_1 + a_2 x_2 \tag{3.3}$$

It is further assumed that R and Y are well determined; therefore, the method of least square analysis given in Reference 8, is applicable to determine the values of the constants, K, n, and m. This analysis was performed using the data given in Tables 3.1 through 3.4 and yielded the equations given below.

For the HF channel data:

$$H_\phi = -\frac{8.28 \times 10^7 Y^{0.522}}{R^{2.23}} \tag{3.4}$$

$$\frac{dH_\phi}{dt} = -\frac{4.84 \times 10^{12} Y^{0.521}}{R^{2.12}} \tag{3.5}$$

$$\frac{dH_r}{dt} = -\frac{1.18 \times 10^{16} Y^{0.385}}{R^{3.46}} \tag{3.6}$$

$$\frac{dH_z}{dt} = -\frac{3.52 \times 10^{16} Y^{0.875}}{R^{3.56}} \tag{3.7}$$

For the LF channel data:

$$H_\phi = -\frac{32.3 Y^{2.16}}{R^{0.813}} \tag{3.8}$$

$$\frac{dH_\phi}{dt} = -\frac{5 \times 10^{12} Y}{R^{2.58}} \tag{3.9}$$

$$\frac{dH_r}{dt} = -\frac{4.91 \times 10^{11} Y^{0.76}}{R^{2.17}} \tag{3.10}$$

Where: Y = yield, kt
R = distance, meters

No significant error is introduced by rounding off the values of the exponents in Equations 3.4 and 3.5 so that these are revised to read, for HF channel data:

$$H_\phi = -\frac{1.8 \times 10^{7} Y^{0.5}}{R^{2}} \tag{3.11}$$

$$\frac{dH_\phi}{dt} = -\frac{2.3 \times 10^{12} Y^{0.5}}{R^{2}} \tag{3.12}$$

These two equations are plotted as solid lines in Figures 3.8 and 3.9. Inspection shows fairly good agreement between the experimental points and these empirical curves. This would indicate that the first peak of azimuthal field as well as first peak of its time derivative could well arise from a vertical electric dipole as assumed in the discussion in Chapter 1. The negative values obtained (with one exception that remains unexplained) further indicate an initially downward flowing current. This is in agreement with the observations of all the other experimenters.

It is noted that the relatively good scaling law agreement between H_ϕ and dH_ϕ/dt as evident from Equations 3.4 and 3.5 does not carry over into their LF components obtained from subsequent peaks. The least-square analyses leading to Equations 3.8 and 3.9 result in widely different yield and range dependence. It must be noted that fewer experimental points were available for these analyses, with considerable scatter. Changing the value of the yield exponent in Equation 3.9 to agree with that of Equation 3.12 results in virtually no change in the range exponent (2.58 to 2.60). For the sake of uniformity and to afford some basis for comparison the yield exponent in Equation 3.8 was similarly changed to 0.5. The resultant equations, replacing 3.8 and 3.9, which were then used for the dashed curves in Figures 3.8 and 3.9 are, for LF channel data:

$$H_\phi = -\frac{3.9 \times 10^{6} Y^{0.5}}{R^{1.8}} \tag{3.13}$$

$$\frac{dH_\phi}{dt} = -\frac{2.3 \times 10^{13} Y^{0.5}}{R^{2.6}} \tag{3.14}$$

The same rounding off procedure used for H_ϕ and dH_ϕ/dt was also used for Equations 3.6

and 3.7, so that these are revised to read, for HF channel data:

$$\frac{dH_r}{dt} = -\frac{1.2 \times 10^{16} Y^{0.4}}{R^{3.5}} \tag{3.15}$$

$$\frac{dH_z}{dt} = -\frac{3.5 \times 10^{16} Y^{0.7}}{R^{3.5}} \tag{3.16}$$

These two equations are plotted as solid lines in Figures 3.10 and 3.11. A vertical electric dipole does not have radial or vertical magnetic fields associated with it, nor is there an inverse cube dependence on the distance on the associated azimuthal field. A horizontal magnetic dipole does, however, have these two components, and the highest power dropoff with distance is the third power. It may, therefore, be postulated that the burst has a more complex electric-magnetic moment than a simple electric dipole and could possibly include a horizontal magnetic dipole.

The value of the yield exponent in Equation 3.10 was changed to 0.4 to agree with the HF channel equation for dH_r/dt, resulting in an expression for LF channel data:

$$\frac{dH_r}{dt} = -\frac{1 \times 10^{13} Y^{0.4}}{R^{2.5}} \tag{3.17}$$

This curve is plotted as the dashed line in Figure 3.10.

The probable error in the yield dependence was investigated for Equation 3.9, which postulated a dependence on yield to the first power. The probable error was found to be ± 0.4, which gives some degree of credence to the rather arbitrary assignment of the yield exponent selected for Equation 3.14.

In summary, the recommended scaling equations for the first peaks (HF data) are 3.11, 3.12, and 3.16 and for the subsequent peaks of the delayed, LF signals, 3.13, 3.14, and 3.17. It must be emphasized that these recommendations (based on one test series involving a rather restricted range of yields, variety of weapon types, and altitudes) are relatively hazardous estimates.

TABLE 3.1 SUMMARY OF AMPLITUDES OF FIRST PEAKS, H_ϕ

Shot	Slant Range	Peak Amplitude	Peak Amplitude / (yield)$^{1/2}$
	meters	ampere turns/meter	ampere turns/meter / kt$^{1/2}$
HF Channels			
Priscilla	938	−183	−30.2
Priscilla	2,200	−20	−3.3
Hood	498	640	74.4
Hood	566	−673	−78.4
Owens	368	−432	−139
Owens	2,901	−4.9	−1.6
Wilson	2,901	−6.0	−1.9
LF Channels			
Priscilla	938	−290	−48
Priscilla	2,200	−145	−24
Hood	566	−2,000	−232
Diablo	298	−9.8	−2.3

TABLE 3.2 SUMMARY OF AMPLITUDES OF FIRST PEAKS, dH_ψ/dt

Shot	Slant Range	Peak Amplitude	Peak Amplitude / (yield)$^{1/2}$
	meters	ampere turns/meter-sec	ampere turns/meter-sec / kt$^{1/2}$
HF Channels			
Priscilla	2,200	-2.5×10^6	-4.1×10^5
Hood	498	-8.9×10^7	-1.0×10^6
Hood	566	-5.7×10^7	-6.7×10^6
Hood	1,590	-2.7×10^6	-3.1×10^5
Hood	2,930	-2.1×10^6	-2.4×10^5
Owens	568	-8.4×10^7	-2.6×10^6
Owens	1,532	-3.9×10^6	-1.3×10^6
Owens	2,901	-5.6×10^5	-1.8×10^5
Wilson	250	-1.2×10^8	-3.7×10^7
Wilson	1,532	-3.3×10^6	-1.0×10^6
Diablo	298	-2.5×10^5	-5.9×10^4
Lassen	250	9.6×10^5	4.4×10^7
LF Channels			
Priscilla	2,200	-3.8×10^5	-1.5×10^5
Hood	566	-1.2×10^7	-4.8×10^6
Wilson	250	-3.8×10^7	-1.2×10^7
Wilson	368	-1.3×10^7	-4.8×10^6
Wilson	1,532	-9.0×10^4	-2.4×10^4
Diablo	298	1.2×10^5	2.8×10^4

TABLE 3.3 SUMMARY OF FIRST PEAK AMPLITUDES, H_r AND H_z

Shot	Slant Range	Peak Amplitude	Peak Amplitude / yield^n
	meters	ampere turns/meter	ampere turns/meter / kt^n
HF Channels, H_r			n = 0.4
Hood	498	−213	−38.0
LF Channels, H_r			n = 0.4
Hood	498	−894	−160
LF Channels, H_z			n = 0.7
Wilson	1,532	−42	−8.2

TABLE 3.4 SUMMARY OF FIRST PEAK AMPLITUDES, dH_r/dt AND dH_z/dt

Shot	Slant Range meters	Peak Amplitude ampere turns/meter-sec	Peak Amplitude / yield[n] ampere turns/meter-sec / kt[n]
HF Channels, dH_r/dt			n = 0.4
Priscilla	938	-2.5×10^6	-9.7×10^5
Hood	498	-2.5×10^7	-4.5×10^6
Hood	1,590	-4.6×10^5	-8.2×10^4
Owens	1,532	-2.4×10^5	-9.7×10^4
LF Channels, dH_r/dt			n = 0.4
Priscilla	938	-2.6×10^6	-6.2×10^5
Owens	1,532	-3.1×10^5	-1.3×10^5
Wilson	776	-1.5×10^6	-5.9×10^5
HF Channels, dH_z/dt			n = 0.7
Priscilla	2,200	-2.8×10^5	-2.3×10^4
Hood	867	-2.5×10^7	-1.2×10^6
Owens	2,901	1.1×10^5	2.3×10^4
Lassen	368	-1.4×10^5	-3.3×10^7
LF Channels, dH_z/dt			n = 0.7
Wilson	1,532	-1.8×10^4	-3.5×10^3

TABLE 3.5 PARTICIPATION AND OSCILLOGRAM REFERENCE, SHOT PRISCILLA

NR, not recorded.

Magnetic Field Component	Station F6.2-9037 .01	.02	.03	.04	.05
H_ϕ	*	†	3.1a, b, c	3.1f, g, h	‡
dH_ϕ/dt			NR	3.1i, j	
H_r			NR	NR	
dH_r/dt			3.1d, e	NR	
H_z			NR	NR	
dH_z/dt			NR	3.1k	

Letters refer to oscillograms in Figures 3.1 through 3.7

* Timing signal failure; no record.

† Recorder failure; no record.

‡ Recorder sensitivity too low; no data.

TABLE 3.6 PARTICIPATION AND OSCILLOGRAM REFERENCE, SHOT HOOD

NR, not recorded.

Magnetic Field Component	Station 9-6.2-9006 .01	.02	.03	.04	.05
H_ϕ	3.2a	3.3a, b, c	NR	3.4a, b‡	NR
dH_ϕ/dt	3.2b, c	3.3d, e	3.3f, g*	3.4c, d§	3.4g
H_r	3.2d, e, f	NR	NR	¶	NR
dH_r/dt	3.2g, h	NR	NR	3.4e, f	NR
H_z	NR	NR	†	NR	**
dH_z/dt	NR	NR	3.3h, i	NR	NR

* LF signal greater than 10^7 ampere turns/meter-sec.
† LF signal greater than 6×10^3 ampere turns/meter-sec.
‡ LF signal greater than 150 ampere turns/meter.
§ LF signal greater than 1.6×10^6 ampere turns/meter-sec.
¶ LF signal greater than 163 ampere turns/meter.
** HF signal greater than 10 ampere turns/meter.

TABLE 3.7 PARTICIPATION AND OSCILLOGRAM REFERENCE, SHOT OWENS

NR, not recorded.

Magnetic Field Component	Station 9-6.2-9006 .02	.04	.05
H_ϕ	3.5a	NR	3.5g
dH_ϕ/dt	3.5b	3.5c	3.5h
H_r	NR	NR	NR
dH_r/dt	NR	3.5d, e, f	NR
H_z	NR	NR	NR
dH_z/dt	NR	NR	3.5i

TABLE 3.8 PARTICIPATION AND OSCILLOGRAM REFERENCE, SHOT WILSON

NR, not recorded.

Magnetic Field Component	Station 9-6.2-9006 .02	.02	.03	.04	.05
H_ϕ	NR			3.6e, f	3.6j
dH_ϕ/dt	3.6a, b	3.6c		NR	†
H_r	NR	NR	NR	NR	NR
dH_r/dt	NR	NR	3.6d	NR	NR
H_z	NR	NR	NR	3.6g, h	NR
dH_z/dt	NR	NR	NR	3.6i*	NR

* HF signal greater than 7×10^5 ampere turns/meter-sec.
† HF signal greater than 5×10^4 ampere turns/meter-sec.

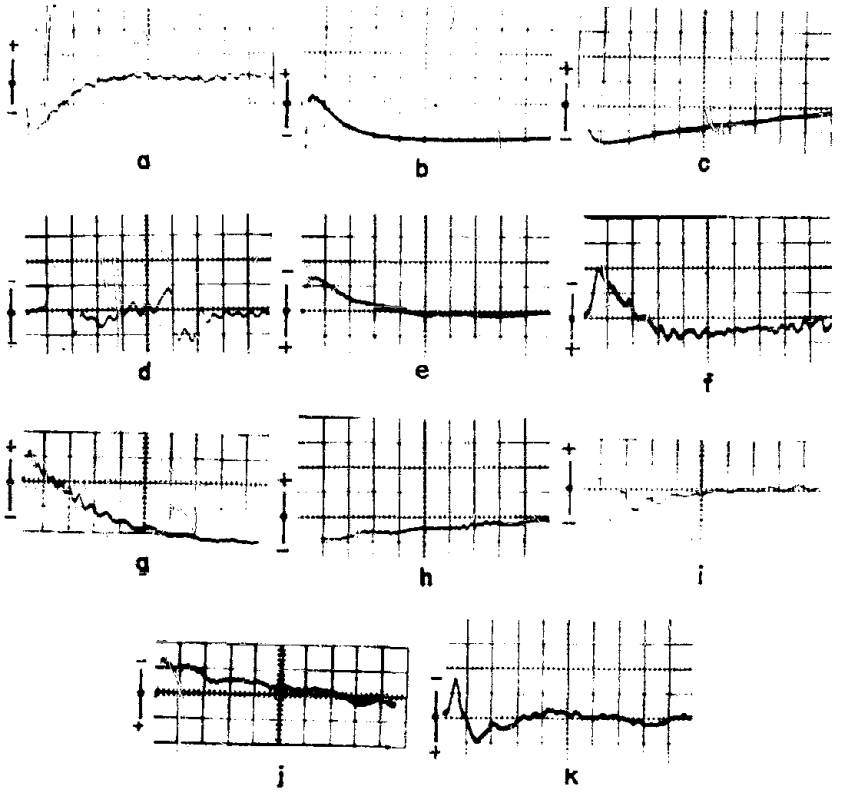

Figure	Station	Component	Horizontal Sensitivity (per division)	Vertical Sensitivity (per division)	
			second	ampere turns/ meter-sec	ampere turns/ meter
3.1a	.03	H_ϕ	10×10^{-6}		73.5
b	.03	H_ϕ*	1×10^{-3}		200
c	.03	H_ϕ*	5×10^{-3}		200
d	.03	dH_r/dt	10×10^{-6}	1.4×10^6	
e	.03	dH_r/dt	1×10^{-3}	1.9×10^6	
f	.04	H_ϕ	10×10^{-6}		11
g	.04	H_ϕ*	500×10^{-6}		160
h	.04	H_ϕ*	5×10^{-3}		160
i	.04	dH_ϕ/dt	5×10^{-6}	1.1×10^6	
j	.04	dH_ϕ/dt*	1×10^{-3}	6.3×10^5	
k	.04	dH_z/dt	10×10^{-6}	1.7×10^5	

*Taken from LF channel.

Figure 3.1 Oscillograms of H and dH/dt versus time, Shot Priscilla.

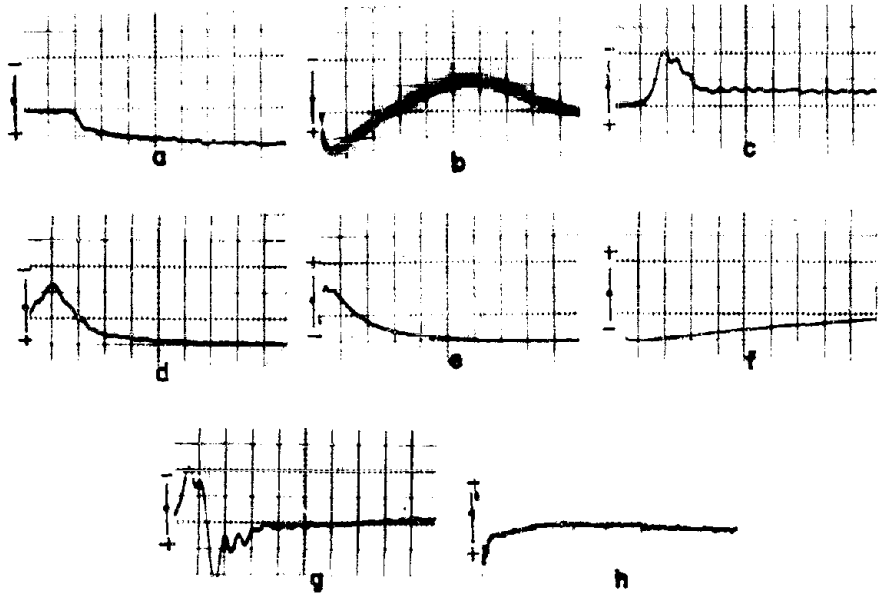

Figure	Station	Component	Horizontal Sensitivity (per division)	Vertical Sensitivity (per division)	
			second	ampere turns/ meter-sec	ampere turns/ meter
3.2a	.01	H_ϕ	100×10^{-6}		460
b	.01	dH_ϕ/dt	100×10^{-6}	4.3×10^7	
c	.01	dH_ϕ/dt	1×10^{-3}	4.3×10^7	
d	.01	H_r	10×10^{-6}		163
e	.01	H_r*	500×10^{-6}		894
f	.01	H_r*	5×10^{-3}		894
g	.01	dH_r/dt	10×10^{-6}	1.4×10^7	
h	.01	dH_r/dt	50×10^{-6}	1.4×10^7	

*Taken from LF channel.

Figure 3.2 Oscillograms of H and dH/dt versus time, Shot Hood.

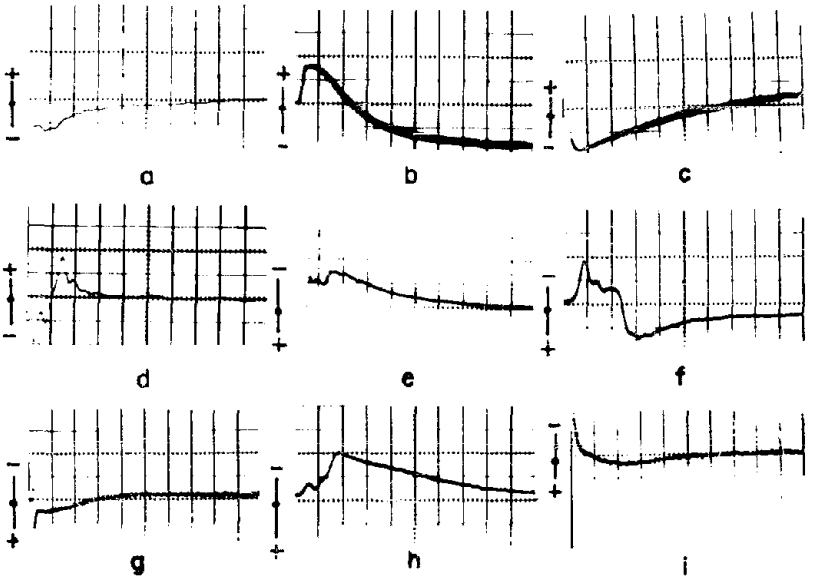

Figure	Station	Component	Horizontal Sensitivity (per division)	Vertical Sensitivity (per division)	
			second	ampere turns/ meter-sec	ampere turns/ meter
3.3a	.02	H_ϕ	10×10^{-6}		518
b	.02	H_ϕ*	500×10^{-6}		1,130
c	.02	H_ϕ*	10×10^{-3}		1,130
d	.02	dH_ϕ/dt	10×10^{-6}	2.7×10^{7}	
e	.02	dH_ϕ/dt*	500×10^{-6}	1×10^{7}	
f	.03	dH_ϕ/dt	10×10^{-6}	1.3×10^{7}	
g	.03	dH_ϕ/dt	1×10^{-3}	1.3×10^{7}	
h	.03	dH_z/dt	10×10^{-6}	1.45×10^{7}	
i	.03	dH_z/dt	1×10^{-3}	1.45×10^{7}	

*Taken from LF channel.

Figure 3.3 Oscillograms of H and dH/dt versus time, Stations .02 and .03, Shot Hood.

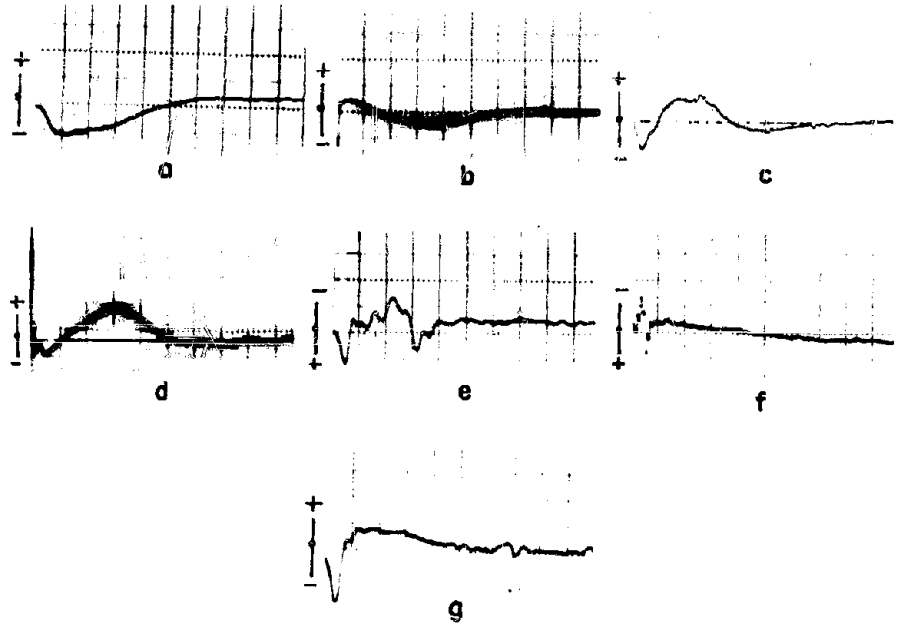

Figure	Station	Component	Horizontal Sensitivity (per division)	Vertical Sensitivity (per division)	
			second	ampere turns/ meter-sec	ampere turns/ meter
3.4a	.04	H_ϕ	10×10^{-6}		37
b	.04	H_ϕ	500×10^{-6}		37
c	.04	dH_ϕ/dt	10×10^{-6}	2.7×10^6	
d	.04	dH_ϕ/dt	500×10^{-6}	2.7×10^6	
e	.04	dH_r/dt	10×10^{-6}	3.8×10^5	
f	.04	dH_r/dt	50×10^{-6}	3.8×10^5	
g	.05	dH_ϕ/dt	10×10^{-6}	1×10^6	

Figure 3.4 Oscillograms of H and dH/dt versus time, Stations .04 and .05, Shot Hood.

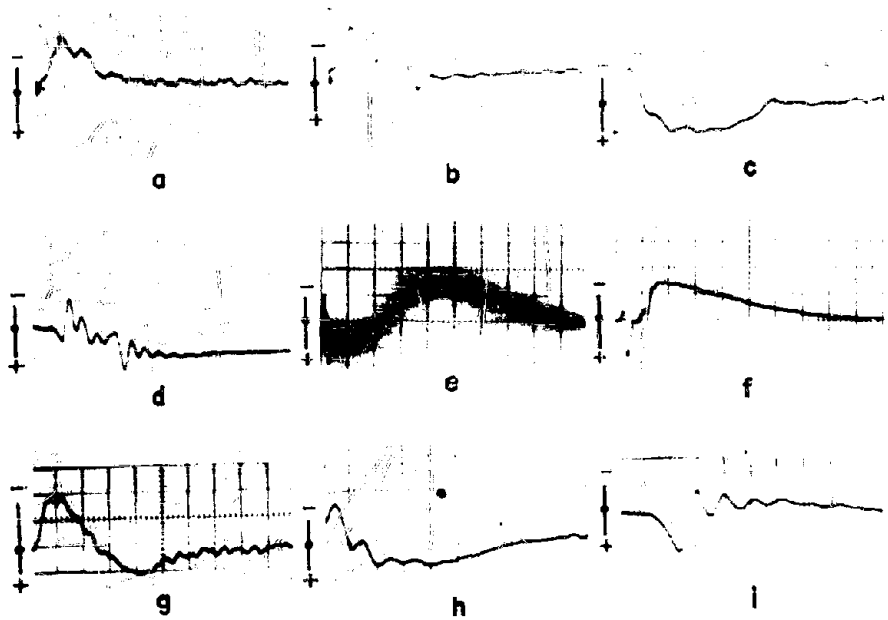

Figure	Station	Component	Horizontal Sensitivity (per division)	Vertical Sensitivity (per division)	
			second	ampere turns/ meter-sec	ampere turns/ meter
3.5a	.02	H_ϕ	5×10^{-6}		216
b	.02	dH_ϕ/dt	5×10^{-6}	4×10^{7}	
c	.04	dH_ϕ/dt	5×10^{-6}	2.8×10^{6}	
d	.04	dH_r/dt	10×10^{-6}	2.4×10^{5}	
e	.04	dH_r/dt	100×10^{-6}	2.4×10^{5}	
f	.05	dH_r/dt*	500×10^{-6}	2.2×10^{5}	
g	.05	H_ϕ	10×10^{-6}		2.7
h	.05	dH_ϕ/dt	5×10^{-6}	4.5×10^{5}	
i	.05	dH_z/dt	5×10^{-6}	7.1×10^{4}	

*Taken from LF channel.

Figure 3.5 Oscillograms of H and dH/dt versus time, Shot Owens.

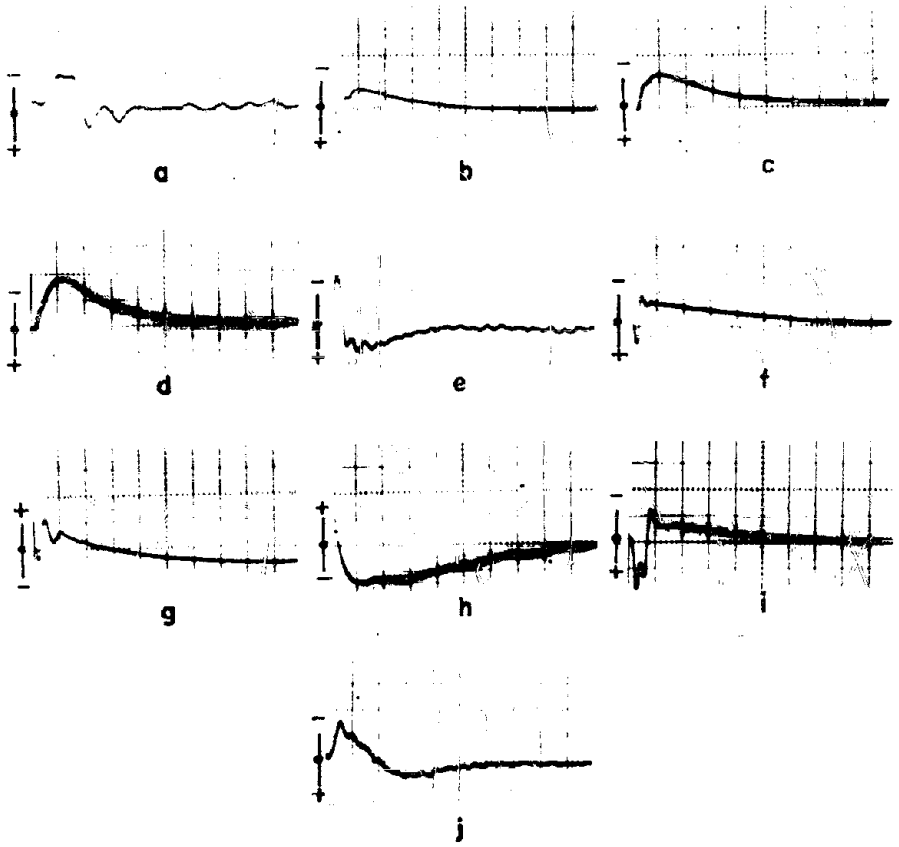

Figure	Station	Component	Horizontal Sensitivity (per division)	Vertical Sensitivity (per division)	
			second	ampere turns/ meter-sec	ampere turns/ meter
3.6a	.01	dH_ϕ/dt	5×10^{-6}	8.5×10^{7}	
b	.01	dH_ϕ/dt*	500×10^{-6}	6.3×10^{7}	
c	.02	dH_ϕ/dt*	500×10^{-6}	1×10^{7}	
d	.03	dH_r/dt*	500×10^{-6}	8.2×10^{5}	
e	.04	dH_ϕ/dt	10×10^{-6}	1.9×10^{6}	
f	.04	dH_ϕ/dt*	500×10^{-6}	1×10^{5}	
g	.04	H_z*	500×10^{-6}		64
h	.04	H_z*	5×10^{-3}		32
i	.04	dH_z/dt*	500×10^{-6}	2.5×10^{4}	
j	.05	H_ϕ	10×10^{-6}		4

*Data from LF channel.

Figure 3.6 Oscillograms of H and dH/dt versus time, Shot Wilson.

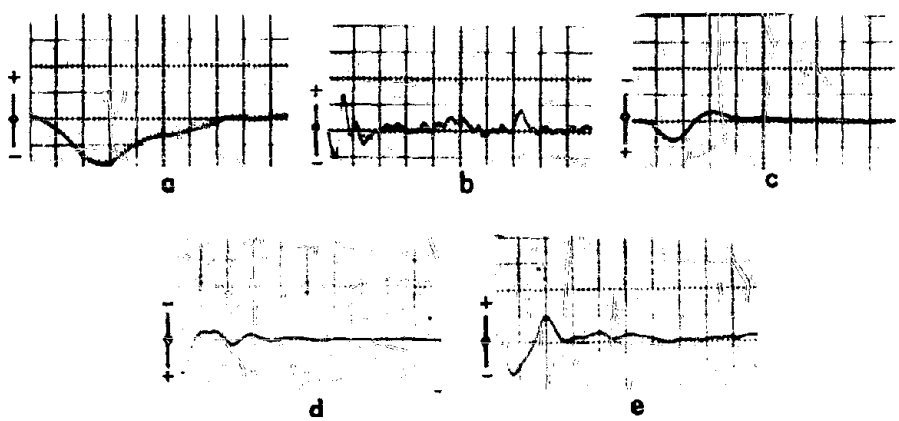

Figure	Station	Component	Horizontal Sensitivity (per division)	Vertical Sensitivity (per division)	
			second	ampere turns/ meter-sec	ampere turns/ meter
Diablo Station, 2B-6.2-900.1					
3.7a		H_ϕ*	100×10^{-6}		5.6
b		dH_ϕ/dt	10×10^{-6}	2.5×10^5	
c		dH_ϕ/dt*	100×10^{-6}	1.8×10^5	
Lassen Station, 9-6.2-9006					
d	.01	dH_ϕ/dt	5×10^{-6}	7.4×10^5	
e	.02	dH_z/dt	5×10^{-6}	1.2×10^5	

*Data taken from LF channel.

Figure 3.7 Oscillograms of H and dH/dt versus time, Shots Diablo and Lassen.

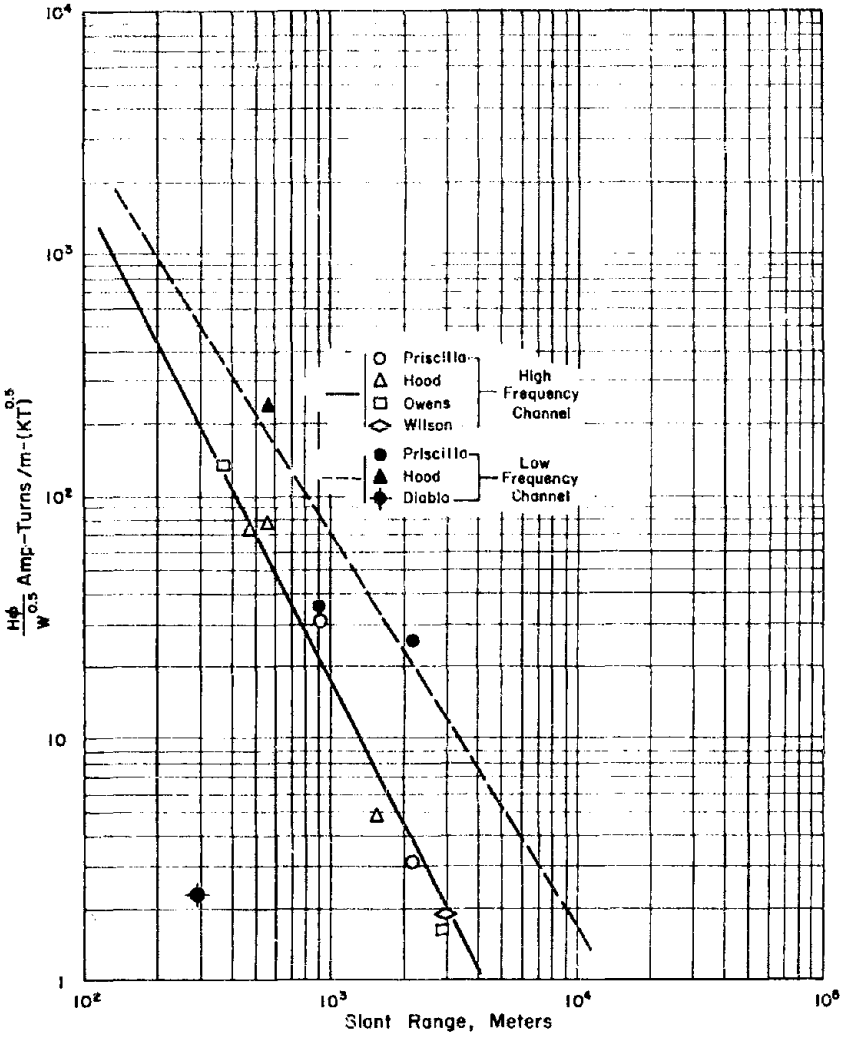

Figure 3.8 Normalized amplitudes versus slant range, H_ϕ.

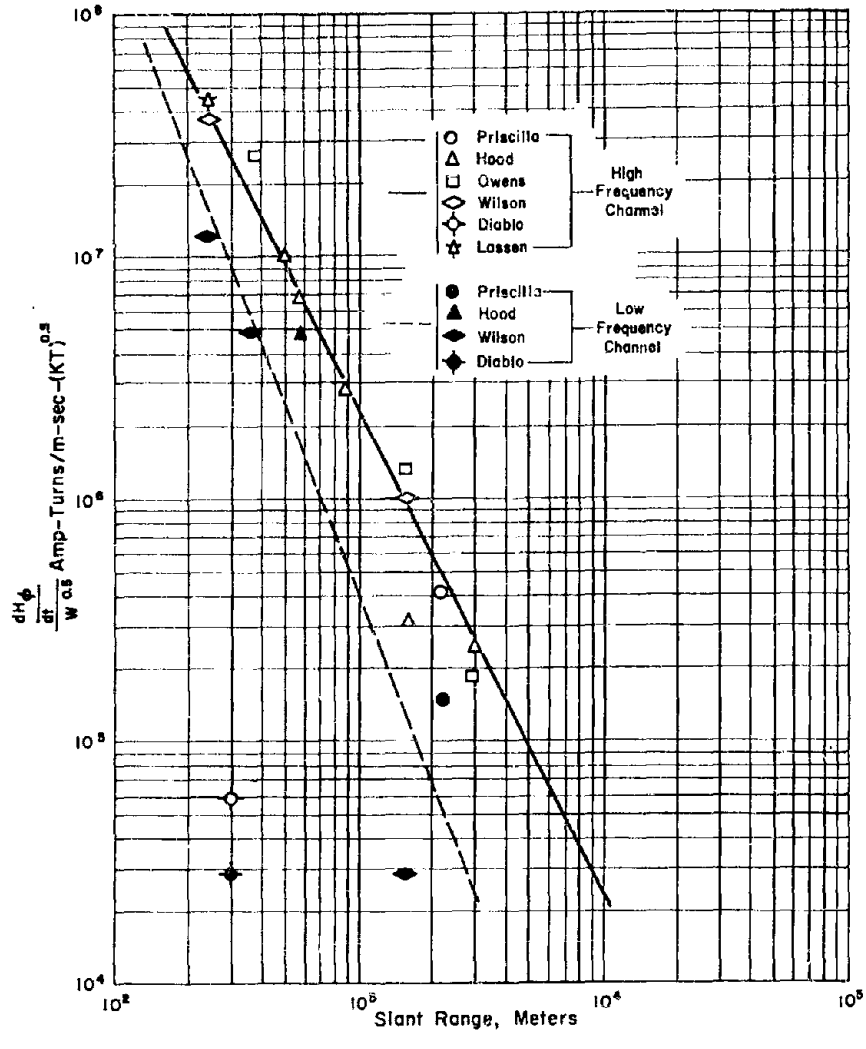

Figure 3.9 Normalized amplitudes versus slant range, dH_ϕ/dt.

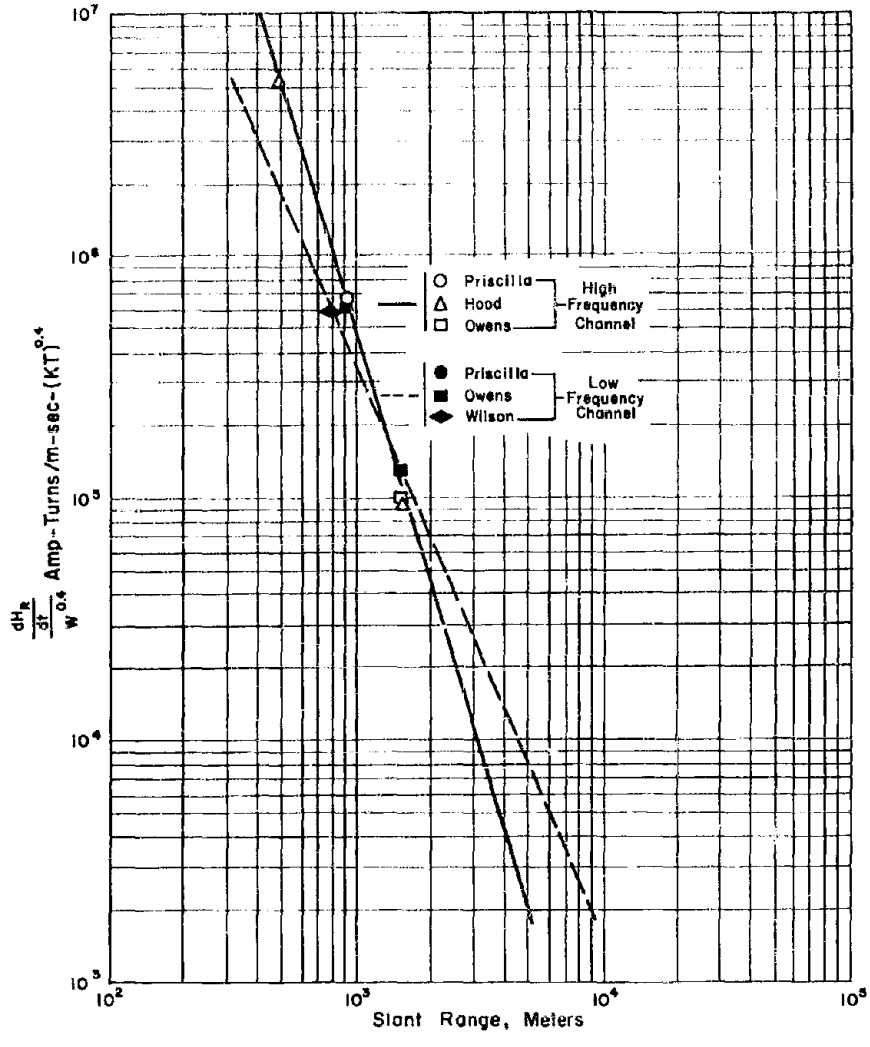

Figure 3.10 Normalized amplitudes versus slant range dH_r/dt.

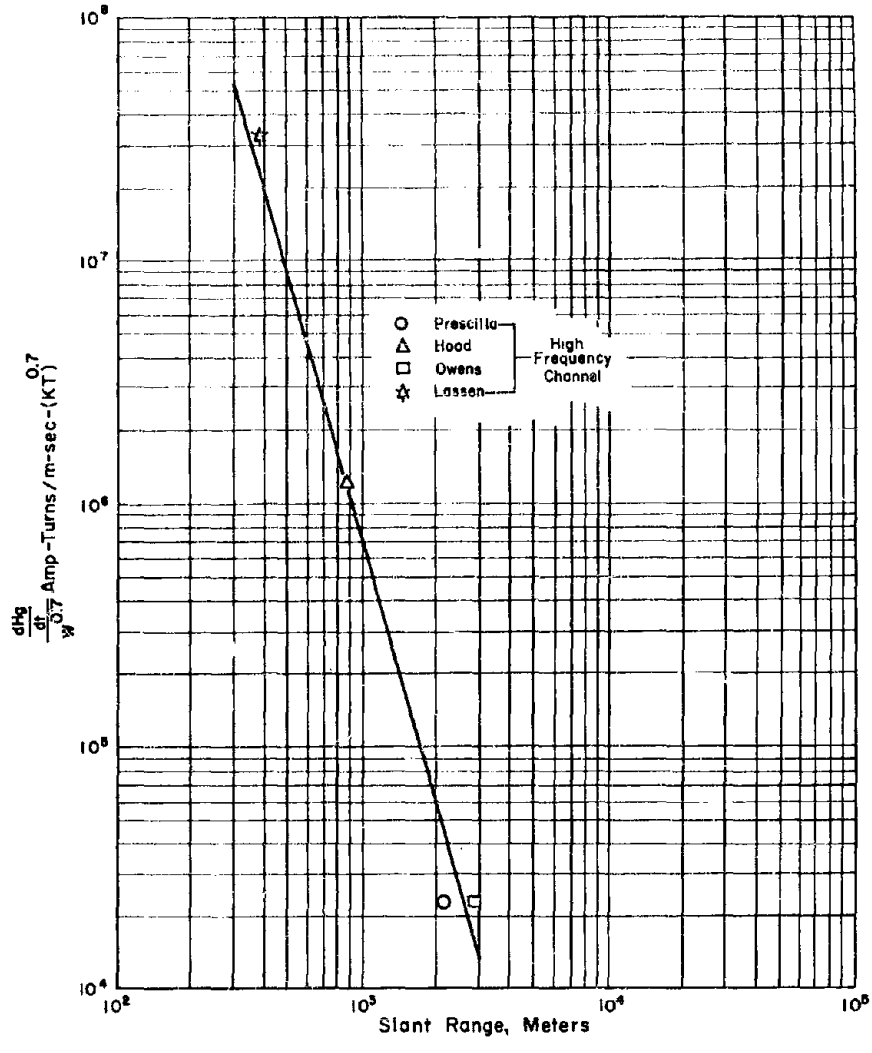

Figure 3.11 Normalized amplitudes versus slant range, dH_z/dt.

Chapter 4

CONCLUSIONS AND RECOMMENDATIONS

4.1 CONCLUSIONS

The magnetic field component of the electromagnetic field in the close vicinity of a nuclear detonation:

(1) consists of both a field rising to an initial peak in a few microseconds and decaying to zero in less than 100 msec as well as a field of considerably longer duration that, at very close distances, appears to coalesce in time with the earlier component, rising to a peak in a few milliseconds and decaying over much longer periods;

(2) has its major component in a horizontal plane, counterclockwise around the detonation point with maximum peak amplitudes of the order of 10^3 ampere turns per meter at distances less than 1,000 meters from the detonation point;

(3) has radial and vertical components whose amplitudes are generally smaller than the major component;

(4) has rise times such that maximum time derivatives of the field are of the order of 10^8 ampere turns per meter per second.

4.2 RECOMMENDATIONS

For more reliable scaling laws, the experiment needs to be repeated on an expanded scale to include higher yield shots, more complete spatial coverage, and more recording channels per station.

REFERENCES

1. R.D. England, and R.E. Partridge, Jr.; "Investigation of Early Electromagnetic Signals"; Project 15.4, Operation Upshot-Knothole, WT-791, November 1953; Los Alamos Scientific Laboratory, Los Alamos, New Mexico; Secret Restricted Data.

2. John S. Malik, and Roger Ray; "Electromagnetic Experiments"; Project 15.2, Operation Castle, WT-949, December 1954; Los Alamos Scientific Laboratory, Los Alamos, New Mexico; Secret Restricted Data.

3. M.H. Oleson; "Electromagnetic Effects of Nuclear Explosions"; Project 7.1, Operation Upshot-Knothole, WT-762, June 1955; Headquarters, U.S. Air Force, AFOAT-1, Washington 25, D.C.; Secret Restricted Data.

4. Roman T. Kowalski, and Charles J. Ong; "Measurement of Radio-Frequency Electromagnetic Radiation from Nuclear Detonations (U)"; Project 6.5, Operation Redwing, WT-1353, March 1960; U.S. Army Signal Engineering Laboratories, Fort Monmouth, New Jersey; Secret Restricted Data.

5. J.P. Wesley; "Theory of Electromagnetic Field from a Ground Shot"; UCRL-5177, July 1958; Lawrence Radiation Laboratory, Livermore, California; Confidential.

6. A.S. Kompaneets; "Radio Emission from an Atomic Explosion"; Soviet Physics JETP, Vol. 35(8), No. 6, pp. 1076-1080, June 1959.

7. John M. Harding, and George E. Baker; "Measurements of Electric Transients in the Earth"; Project 15.2, Operation Upshot-Knothole, WT-813, December 1953; Sandia Corporation, Albuquerque, New Mexico; Confidential Restricted Data.

8. Mengel; "Fundamental Formulas of Physics"; Vol. I, p. 124; Dover Publications.

DISTRIBUTION

Military Distribution Category 62

ARMY ACTIVITIES

1 Deputy Chief of Staff for Military Operations, D/A, Washington 25, D.C. ATTN: Dir. of SW&R
2 Chief of Research and Development, D/A, Washington 25, D.C. ATTN: Atomic Div.
3 Assistant Chief of Staff, Intelligence, D/A, Washington 25, D.C.
4 Chief of Engineers, D/A, Washington 25, D.C. ATTN: ENGNB
5 Chief of Engineers, D/A, Washington 25, D.C. ATTN: ENGTN
6- 7 Office, Chief of Ordnance, D/A, Washington 25, D.C. ATTN: ORDTK
8 Chief Signal Officer, D/A, Research and Development Div., Washington 25, D.C. ATTN: SIGRD-4
9- 11 Commanding General, U.S. Continental Army Command, Ft. Monroe, Va.
12 Director of Special Weapons Development Office, Headquarters CONARC, Ft. Bliss, Tex. ATTN: Capt. Chester I. Peterson
13 President, U.S. Army Artillery Board, Ft. Sill, Okla.
14 President, U.S. Army Air Defense Board, Ft. Bliss, Tex.
15 President, U.S. Army Aviation Board, Ft. Rucker, Ala. ATTN: ATBG-DG
16 Commandant, U.S. Army Command & General Staff College, Ft. Leavenworth, Kansas. ATTN: ARCHIVES
17 Commandant, U.S. Army Air Defense School, Ft. Bliss, Tex. ATTN: Command & Staff Dept.
18 Commandant, U.S. Army Armored School, Ft. Knox, Ky.
19 Commandant, U.S. Army Artillery and Missile School, Ft. Sill, Okla. ATTN: Combat Development Department
20 Commandant, U.S. Army Aviation School, Ft. Rucker, Ala.
21 Commandant, U.S. Army Infantry School, Ft. Benning, Ga. ATTN: C.D.S.
22 Commanding General, Chemical Corps Training Comd., Ft. McClellan, Ala.
23 Commanding Officer, U.S. Army Research Lab., Ft. Knox, Ky.
24 Commanding General, U.S. Army Chemical Corps, Research and Development Comd., Washington 25, D.C.
25 Commanding Officer, Chemical Warfare Lab., Army Chemical Center, Md. ATTN: Tech. Library
26 Commanding Officer, Diamond Ord. Fuze Labs., Washington 25, D.C. ATTN: Chief, Nuclear Vulnerability Br. (240)
27 Commanding General, Aberdeen Proving Grounds, Md. ATTN: Director, Ballistics Research Laboratory
28- 29 Commanding General, U.S. Army Ord. Missile Command, Redstone Arsenal, Ala.
30 Commander, Army Rocket and Guided Missile Agency, Redstone Arsenal, Ala. ATTN: Tech Library
31 Commanding General, White Sands Missile Range, N. Mex. ATTN: ORDBS-OM-TL
32 Commander, Army Ballistic Missile Agency, Redstone Arsenal, Ala. ATTN: ORDAB-HT
33 Commanding General, Ordnance Ammunition Command, Joliet, Ill.
34 Commanding Officer, USA Signal R&D Laboratory, Ft. Monmouth, N.J.
35 Commanding General, U.S. Army Electronic Proving Ground, Ft. Huachuca, Ariz. ATTN: Tech. Library
36 Commanding General, USA Combat Surveillance Agency, 1125 N. Highland St., Arlington, Va.
37 Commanding Officer, USA, Signal R&D Laboratory, Ft. Monmouth, N.J. ATTN: Tech. Doc. Ctr., Evans Area
38 Director, Operations Research Office, Johns Hopkins University, 6935 Arlington Rd., Bethesda 14, Md.

NAVY ACTIVITIES

39- 40 Chief of Naval Operations, D/N, Washington 25, D.C. ATTN: OP-03EG
41 Chief of Naval Operations, D/N, Washington 25, D.C. ATTN: OP-75
42 Chief of Naval Operations, D/N, Washington 25, D.C. ATTN: Op-347G1
43- 44 Chief of Naval Research, D/N, Washington 25, D.C. ATTN: Code 811
45- 47 Chief, Bureau of Naval Weapons, D/N, Washington 25, D.C. ATTN: DLI-3
48 Chief, Bureau of Ordnance, D/N, Washington 25, D.C.
49 Chief, Bureau of Ships, D/N, Washington 25, D.C. ATTN: Code 423
50 Director, U.S. Naval Research Laboratory, Washington 25, D.C. ATTN: Mrs. Katherine H. Cass
51- 52 Commander, U.S. Naval Ordnance Laboratory, White Oak, Silver Spring 19, Md.
53 Commanding Officer and Director, Navy Electronics Laboratory, San Diego 52, Calif.
54 Commanding Officer, U.S. Naval Mine Defense Lab., Panama City, Fla.
55 Commanding Officer, U.S. Naval Radiological Defense Laboratory, San Francisco, Calif. ATTN: Tech. Info. Div.
56 Commanding Officer and Director, U.S. Naval Civil Engineering Laboratory, Port Hueneme, Calif. ATTN: Code L31
57 Commanding Officer, U.S. Naval Schools Command, U.S. Naval Station, Treasure Island, San Francisco, Calif.
58 Superintendent, U.S. Naval Postgraduate School, Monterey, Calif.
59 Commanding Officer, Air Development Squadron 5, VX-5, China Lake, Calif.
60 Commandant, U.S. Marine Corps, Washington 25, D.C. ATTN: Code AO3H
61 Director, Marine Corps Landing Force, Development Center, MCS, Quantico, Va.
62 Commanding Officer, U.S. Naval CIC School, U.S. Naval Air Station, Glynco, Brunswick, Ga.
63 Chief of Naval Operations, Department of the Navy, Washington 25, D.C. ATTN: OP-05E2
64- 66 Chief, Bureau of Naval Weapons, Navy Department, Washington 25, D.C. ATTN: RRRE

AIR FORCE ACTIVITIES

67 Air Force Technical Application Center, HQ. USAF, Washington 25, D.C.
68 Hq. USAF, ATTN: Operations Analysis Office, Office, Vice Chief of Staff, Washington 25, D. C.
69 Director of Civil Engineering, HQ. USAF, Washington 25, D.C. ATTN: AFOCE-ES
70- 74 HQ. USAF, Washington 25, D.C. ATTN: AFCIN-3D1
75 Director of Research and Development, DCS/D, HQ. USAF, Washington 25, D.C. ATTN: Guidance and Weapons Div.
76 Commander, Tactical Air Command, Langley AFB, Va. ATTN: Doc. Security Branch
77 Commander, Air Defense Command, Ent AFB, Colorado. ATTN: Operations Analysis Section, ADCOA
78 Commander, Hq. Air Research and Development Command, Andrews AFB, Washington 25, D.C. ATTN: RDRWA
79 Commander, Air Force Ballistic Missile Div. HQ. ARDC, Air Force Unit Post Office, Los Angeles 45, Calif. ATTN: WDSOT
80 Commander, Second Air Force, Barksdale AFB, La. ATTN: Operations Analysis Office
81- 83 Commander, AF Cambridge Research Center, L. G. Hanscom Field, Bedford, Mass. ATTN: CRRST-2
84- 85 Commander, Air Force Special Weapons Center, Kirtland AFB, Albuquerque, N. Mex. ATTN: Tech. Info. & Intel. Div.

SECRET

86 Commandant, School of Aviation Medicine, USAF Aerospace Medical Center (ATC), Brooks AFB, Tex. ATTN: Col. G. L. Hoklunis

87- 89 Commander, Wright Air Development Center, Wright-Patterson AFB, Dayton, Ohio. ATTN: WCACT (For WCOSI)

90- 91 Director, USAF Project RAND, VIA: USAF Liaison Office, The RAND Corp., 1700 Main St., Santa Monica, Calif.

92 Commander, Air Defense Systems Integration Div., L. G. Hanscom AFB, Bedford, Mass. ATTN: SAMSO

93 Chief, Ballistic Missile Early Warning Project Office, L. G. Hanscom AFB, Bedford, Mass. ATTN: Col. Leo V. Skinner, USAF

94 Commander, Rome Air Development Center, ARDC, Griffiss AFB, N.Y. ATTN: Documents Library, RCSSL-1

95 Commander, Air Technical Intelligence Center, USAF, Wright-Patterson AFB, Ohio. ATTN: AFCIN-4Bls, Library

96 Headquarters, 1st Missile Div., USAF, Vandenberg AFB, Calif. ATTN: Operations Analysis Office

OTHER DEPARTMENT OF DEFENSE ACTIVITIES

97 Director of Defense Research and Engineering, Washington 25, D.C. ATTN: Tech. Library

98 Director, Weapons Systems Evaluation Group, Room 1E880, The Pentagon, Washington 25, D.C.

99-102 Chief, Defense Atomic Support Agency, Washington 25, D.C. ATTN: Document Library

103 Commander, Field Command, DASA, Sandia Base, Albuquerque, N. Mex.

104 Commander, Field Command, DASA, Sandia Base, Albuquerque, N. Mex. ATTN: FCTO

105-106 Commander, Field Command, DASA, Sandia Base, Albuquerque, N. Mex. ATTN: FCWT

107 Commander-in-Chief, Strategic Air Command, Offutt AFB, Neb. ATTN: OAWS

108 U.S. Documents Officer, Office of the United States National Military Representative - SHAPE, APO 55, New York, N.Y.

ATOMIC ENERGY COMMISSION ACTIVITIES

109-111 U.S. Atomic Energy Commission, Technical Library, Washington 25, D.C. ATTN: For IMA

112-113 Los Alamos Scientific Laboratory, Report Library, P.O. Box 1663, Los Alamos, N. Mex. ATTN: Helen Redman

114-118 Sandia Corporation, Classified Document Division, Sandia Base, Albuquerque, N. Mex. ATTN: H. J. Smyth, Jr.

119-128 University of California Lawrence Radiation Laboratory, P.O. Box 808, Livermore, Calif. ATTN: Clovis G. Craig

129 Division of Technical Information Extension, Oak Ridge, Tenn. (Master)

130-160 Division of Technical Information Extension, Oak Ridge, Tenn. (Surplus)

ADDITIONAL DISTRIBUTION

161-164 Commander, AF Ballistic Missile Div., HQ, ARDC, AF Unit Post Office, Los Angeles 45, Calif. ATTN: WDGWT

165-167 Commander, Rome Air Development Center, ARDC, Griffiss AFB, N.Y. ATTN: Documents Library, RCSSLD

168 Commander, Air Materiel Command, Wright-Patterson AFB, Ohio. ATTN: MCRW

169-170 Chief, Bureau of Ordnance, D/N, Washington 25, D.C. ATTN: SP

171 Director, Defense Communications Agency, Washington 25, D.C.

172 Chief of Naval Operations, D/N, Washington, D.C. ATTN: OP-07

173 Director, Advanced Research Projects Agency, ATTN: Mr. Alvin Van Every, Lt. Col. Roy Neidiger, Dr. C. W. Cook

174 Chief of Research and Development, Dept. of the Army, Washington, D.C. ATTN: Lt. Col. R. L. Conoly, Maj. D. Baker

175 Chief of Naval Research, D/N, Washington 25, D.C. ATTN: Dr. W. J. Thaler

176 OAR, Bldg. T-D, Washington 25, D.C. ATTN: Maj. E. Mangin

177 Commanding Officer, Diamond Ordnance Fuze Laboratories, Connecticut and Van Ness, N.W., Washington 25, D.C. ATTN: J. W. Seaton, Peter Hows

178 Chief, Bureau of Naval Weapons, D/N, Washington 25, D.C. ATTN: Mr. James M. Lee

179 Commanding Officer, U.S. Army Signal Research and Development Lab., Ft. Monmouth, N.J. ATTN: Mr. R. Kulinyi, Mr. L. Kaplan

180 Commander, U.S. Naval Ordnance Lab., White Oak, Silver Spring 19, Md. ATTN: Dr. R. W. Anderson

181 Commanding Officer and Director, U.S. Navy Electronics Lab., San Diego 52, Calif. ATTN: Dr. T. J. Keary

182 Director, U.S. Naval Research Lab., Washington 25, D.C. ATTN: Mr. Irving H. Page

183 AFCRL, L. G. Hanscom AFB, Mass. ATTN: Dr. G. Gassman, Dr. P. Newman, Mr. E. Levin

184 AFSWC, Kirtland AFB, N. Mex. ATTN: Capt. J. Welch, Lt. Col. F. Gross

185 Mr. J. A. Pierce, 311 Cruft Lab., Harvard University, Cambridge, Mass.

186 Director, Lincoln Lab., Mass. Inst. of Technology, P.O. Box 73, Lexington 73, Mass. ATTN: Mr. J. Chisholm

187 Director, Stanford Research Inst., Menlo Park, Calif. ATTN: Dr. R. Leadabrand, Dr. A. Peterson

188 Chief, U.S. Army Signal Radio Propagation Agency, Ft. Monmouth, N.J. ATTN: Mr. Fred Dickson

189 Dr. F. D. Benedict, Bell Telephone Labs., Murray Hill, N.J.

190 WADD, Wright-Patterson AFB, Ohio. ATTN: Lt. Col. V. Bryson

191 Sandia Corp., Sandia Base, Albuquerque, N. Mex. ATTN: Dr. C. Broyles

192 Boeing Airplane Co., 7755 E. Marginal Way, Seattle 8, Wash. ATTN: Dr. D. Hicks

193 Hughes Aircraft Co., Florence and Teale Sts., Culver City, Calif. ATTN: Mrs. T. Benedetto

194 Director of Military Application, U.S. Atomic Energy Commission, Washington, D.C. ATTN: Mr. H. H. Smith

Defense Special Weapons Agency
6801 Telegraph Road
Alexandria, Virginia 22310-3398

TRC

21 August 1997

MEMORANDUM FOR DEFENSE TECHNICAL INFORMATION CENTER
ATTENTION: OMI/Mr. William Bush

SUBJECT: Declassification of AD-336550 and Withdrawal of AD-B951750

The Defense Special Weapons Agency Security Office (OPSSI) has reviewed and declassified the following report:

AD-336550 (WT-1436)
Operation PLUMBBOB, Project 6.2, Measurement of the Magnetic Component of the Electromagnetic Field Near A Nuclear Detonation, Issuance date: May 8, 1962.

Distribution statement **"A"** (approved for public release) now applies.

Since AD-336550 is now declassified and approved for public release, this office requests the extracted version (AD-B951750, WT-1436-EX) be destroyed because it is no longer applicable.

Completed 23 may 2000

for MARDITH JARRETT
Chief, Technical Resource Center

copy furn: FC/DASIAC
KSC/Alex

Completed
7 Jun 2000
BW